

# The primordial abundance of $^4\text{He}$ : a self-consistent empirical analysis of systematic effects in a large sample of low-metallicity H II regions

Yuri I. Izotov

*Main Astronomical Observatory, Ukrainian National Academy of Sciences, 27 Zabolotnoho str., Kyiv 03680, Ukraine*

izotov@mao.kiev.ua

Trinh X. Thuan

*Astronomy Department, University of Virginia, Charlottesville, VA 22903*

txt@virginia.edu

and

Grażyna Stasińska

*LUTH, Observatoire de Meudon, F-92195 Meudon Cedex, France*

grazyna.stasinska@obspm.fr

## ABSTRACT

We determine the primordial helium mass fraction  $Y_p$  using 93 spectra of 86 low-metallicity extragalactic H II regions. This sample constitutes the largest and most homogeneous high-quality data sets in existence for the determination of  $Y_p$ . For comparison and to improve the statistics in our investigation of systematic effects affecting the  $Y_p$  determination, we have also considered a sample of 271 low-metallicity H II regions selected from the Data Release 5 of the Sloan Digital Sky Survey. Although this larger sample shows more scatter, it gives results that are consistent at the  $2\sigma$  level with our original sample. We have considered known systematic effects which may affect the  $^4\text{He}$  abundance determination. They include different sets of He I line emissivities and reddening laws, collisional and fluorescent enhancements of He I recombination lines, underlying He I stellar absorption lines, collisional excitation of hydrogen lines, temperature and ionization structure of the H II region, and deviation of He I and H emission line intensities from case B. However, the most likely value of  $Y_p$  depends on the

adopted set of He I line emissivities. Using Monte Carlo methods to solve simultaneously the above systematic effects we find a primordial helium mass fraction  $Y_p = 0.2472 \pm 0.0012$  when using the He I emissivities from Benjamin et al. (1999, 2002) and  $0.2516 \pm 0.0011$  when using those from Porter et al. (2005). The first value agrees well with the value given by Standard Big Bang Nucleosynthesis (SBBN) theory, while the value obtained with likely more accurate emissivities of Porter et al. (2005) is higher at the  $2\sigma$  level. This latter value, if confirmed, would imply slight deviations from SBBN.

*Subject headings:* galaxies: abundances — galaxies: irregular — galaxies: ISM — H II regions — ISM: abundances

## 1. INTRODUCTION

In the standard theory of big bang nucleosynthesis (SBBN), given the number of light neutrino species, the abundances of these light elements depend only on one cosmological parameter, the baryon-to-photon number ratio  $\eta$ , which in turn is directly related to the baryon density parameter  $\Omega_b$ , the present ratio of the baryon mass density to the critical density of the Universe. This means that accurate measurements of the primordial abundances of each of the four light elements can provide, in principle, a direct measurement of the baryonic density. As  $\eta$  is a very small quantity, it is convenient to define the parameter  $\eta_{10} = 10^{10} \eta$ . Then  $\eta_{10}$  is related to  $\Omega_b$  by the expression  $\eta_{10} = 274 \Omega_b h^2$ , where  $h = H_0/100 \text{ km s}^{-1} \text{ Mpc}^{-1}$  and  $H_0$  is the present value of the Hubble parameter (Steigman 2005).

Because of the strong dependence of its abundance on  $\eta$ , deuterium has become the baryometer of choice ever since accurate measurement of D/H in high-redshift low-metallicity QSO Ly $\alpha$  absorption systems have become possible. Although the data is still scarce – there are only six absorption systems for which such a D/H measurement has been carried out (Burles & Tytler 1998a,b; O’Meara et al. 2001, 2006; Pettini & Bowen 2001; Kirkman et al. 2003; Crighton et al. 2004) – and the scatter remains large, the measurements appear to converge to a mean primordial value  $\text{D/H} \sim 2.4 \pm 0.4 \times 10^{-5}$ , which corresponds to  $\Omega_b h^2 \sim 0.023 \pm 0.002$ . This estimate of  $\Omega_b h^2$  is in excellent agreement with the values of 0.022 – 0.023 obtained from recent studies of the fluctuations of the cosmic microwave background (CMB) by DASI (Pryke et al. 2002), BOOMERANG (Netterfield et al. 2002) and WMAP (Spergel et al. 2003, 2006). It is also in good agreement with the value of  $\Omega_b h^2$  derived from large scale structure (Tegmark et al. 2004).

While a single good baryometer like D is sufficient to derive the baryonic mass den-

sity from BBN, accurate measurements of the primordial abundances of at least two different relic elements are required to check the consistency of SBBN. Among the remaining relic elements,  $^3\text{He}$  can only be observed in the solar system and in the Galaxy, both of which have undergone significant chemical evolution, making it difficult to derive its primordial abundance (Bania et al. 2002). The derivation of the primordial  $^7\text{Li}$  abundance in metal-poor halo stars in the Galaxy is also beset by difficulties such as the uncertain stellar temperature scale and the temperature structures of the atmospheres of these very cool stars (Charbonnel & Primas 2005). The primordial abundance of the remaining relic element,  $^4\text{He}$  (hereafter He), can in principle be derived accurately from observations of the helium and hydrogen emission lines from low-metallicity blue compact dwarf (BCD) galaxies which have undergone little chemical evolution. Several groups have used this technique to derive the primordial He mass fraction  $Y_p$ , with somewhat different results. Our group (Izotov, Thuan & Lipovetsky 1997; Izotov & Thuan 1998b, 2004) has obtained  $Y_p = 0.244 \pm 0.002$ . This value is consistent at the two-sigma level with the prediction of SBBN,  $Y_p = 0.2482 \pm 0.0007$  (Walker et al. 1991; Steigman 2005), adopting the value of  $\Omega_b h^2 = 0.0223 \pm 0.0008$  found by WMAP (Spergel et al. 2006). On the other hand, the  $Y_p$  predicted by SBBN is not consistent with the lower values of  $0.234 \pm 0.002$  derived by Olive et al. (1997), of  $0.2384 \pm 0.0025$  by Peimbert et al. (2002) and of  $0.2391 \pm 0.0020$  by Luridiana et al. (2003). These lower estimates of  $Y_p$  have led some authors to argue that the discrepancy between the  $\Omega_b$ s derived from  $Y_p$  and from D/H is a sign that SBBN is not valid (Chen et al. 2001; Kneller et al. 2001; Barger et al. 2003a,b; Cyburt et al. 2005) and that new physics are required. Although He is not a sensitive baryometer ( $Y_p$  depends only logarithmically on the baryon density), its primordial abundance depends much more sensitively on the expansion rate of the Universe and on a possible asymmetry between the numbers of neutrinos and anti-neutrinos in the early universe than D,  $^3\text{He}$  or  $^7\text{Li}$ . This, because of two reasons: 1) a faster expansion would leave less time for neutrons to convert into protons, and the resulting higher neutron abundance would result in a higher  $Y_p$ , and 2)  $Y_p$  depends sensitively on the neutron to proton ratio, which depends in turn on the numbers of electron neutrinos and anti-neutrinos. In that sense, He is both a chronometer and/or leptometer which is very sensitive to any small deviation from SBBN, and hence to new physics, much more so than the other three primordial light elements (Steigman 2006).

However, to detect small deviations from SBBN and make cosmological inferences,  $Y_p$  has to be determined to a level of accuracy of less than one percent. This is not an easy task. While it is relatively straightforward to derive the helium abundance in an H II region with an accuracy of 10 percent if the spectrum is adequate, gaining one order of magnitude in the precision requires many conditions to be met. First, the observational data has to be of excellent quality. This has been the concern of our group (Izotov, Thuan & Lipovetsky 1994,

1997; Izotov & Thuan 1998b, 2004). We have spent the last decade obtaining high signal-to-noise spectroscopic data of low-metallicity extragalactic H II regions, and our sample includes now a total of 86 H II regions in 77 galaxies (see Izotov & Thuan 2004). This constitutes by far the largest sample of high-quality data reduced in a homogeneous way to investigate the problem of the primordial helium abundance. To put things in perspective, the sample used in the pioneering work of Peimbert & Torres-Peimbert (1974, 1976) comprised only 5 objects, with considerably larger observational errors. Later, the sample of Pagel et al. (1992) included 36 objects and that of Olive & Steigman (1995) 49 objects.

With such a large observational sample at hand, it is now the general consensus that the accuracy of the determination of the primordial He abundance is limited presently, not so much by statistical uncertainties, but by our ability to account for systematic errors and biases. There are many known effects we need to correct for to transform the observed He I line intensities into a He abundance. Neglecting or misestimating them may lead to systematic errors in the  $Y_p$  determination that are larger than the statistical errors. These effects are: (1) reddening, (2) underlying stellar absorption in the He I lines, (3) collisional excitation of the He I lines which make their intensities deviate from their recombination values, (4) fluorescence of the He I lines which also make their intensities deviate from their recombination values, (5) collisional excitation of the hydrogen lines (hydrogen enters because the helium abundance is calculated relative to that of hydrogen), (6) possible departures from case B in the emissivities of H and He I lines, (7) the temperature structure of the H II region and (8) its ionization structure. All these corrections are at a level of a few percent except for effect (3) that can be much higher, exceeding 10% in the case of the He I  $\lambda 5876$  emission line in hot and dense H II regions. All effects, apart from (8), influence each other in a complicated way. At the present time, we are far from a situation where all these corrections can be determined unambiguously from observational constraints and theory. Given the complexity of H II regions – they have very perturbed morphologies, possess complex velocity fields and a dust distribution difficult to quantify – the situation is not likely to be improved considerably in the near future. Because of this, even if one were able to solve in an exact manner the radiation transfer in the case of a simple geometry, there is still a long way between a simple model and a real H II region.

Effects (1), (3), (4) are relatively easy to account for empirically from the available spectroscopic information and have been already considered in the pioneering study of Peimbert & Torres-Peimbert (1974). Corrections (2) and (5) have been discussed more recently (Rayo et al. 1982; Kunth & Sargent 1983; Davidson & Kinman 1985). Effect (7) has been the subject of many papers by Peimbert and his coworkers. Elemental abundance determinations are affected by biases in the presence of temperature inhomogeneities in the H II regions. Peimbert (1967) and Peimbert et al. (2002) have devised an empirical method

to correct for this bias. However, this method relies on several assumptions that are not necessarily valid (e.g. supposing that the temperature fluctuation parameter is the same in the high and low ionization regions, Peimbert et al. 2002). Furthermore, the source of temperature inhomogeneities at the level invoked by Peimbert and colleagues remains unidentified (Stasińska & Schaerer 1999; Binette & Luridiana 2000; Mathis 1995), unless they are supposed to result from abundance inhomogeneities (Tsamis & Péquignot 2005, Stasińska et al., in preparation). This is also why the computation of temperature corrections from photoionization models to derive He/H (as proposed by Sauer & Jedamzik 2002), is not necessarily relevant to real objects. To check for possible temperature fluctuations, Guseva et al. (2006, 2007) have compared the temperature in the  $O^{2+}$  zone derived with the [O III]  $\lambda 4363$  line, with that in the  $H^+$  zone derived with the Balmer and Paschen jumps in a large sample of hot low-metallicity H II regions used in the determination of  $Y_p$ . They found that the two temperatures do not differ statistically, so that any temperature difference must be less than  $\sim 5\%$ . Effect (8) has first been corrected for using an empirical method (Peimbert & Torres-Peimbert 1974), and has been later the subject of many papers based on photoionization modeling (Stasińska 1980; Peña 1986; Viegas et al. 2000; Ballantyne et al. 2000; Sauer & Jedamzik 2002; Gruenwald et al. 2002). Effect (6) has been discussed for H II regions by Cota & Ferland (1988) and Hummer & Storey (1992), but has never been considered in the various estimates of  $Y_p$  thus far, case B having been assumed by all authors.

In the present determination of the primordial He abundance, we take into account all eight effects discussed above. We first use an empirical method to self-consistently account for effects 1, 2, 3, 4, 5 and 7 in the derivation of the abundance of  $He^+$ . This method has been detailed in Izotov & Thuan (2004), where it has been applied to a small sample of 7 objects. It was shown that taking all these effects into account in a systematic way can lead to helium abundances that are significantly higher than those obtained by Peimbert et al. (2002) for the same objects (by up to 3%). Here, we apply the same method, not only to our basic original sample of 93 H II regions (Izotov & Thuan 2004) that we have assembled and observed ourselves (hereafter the HeBCD sample), but also to a different and larger sample of 271 extragalactic H II regions selected from the Data Release 5 (DR5) of the Sloan Digital Sky Survey (hereafter the SDSS sample). We then considered effects 6 and 8 on the derivation of the abundance of He in each H II region and of the primordial He abundance.

We describe the two HeBCD and SDSS samples in §2. In §3 we discuss the method used to derive He abundances in individual objects and the primordial He abundance from each sample. In §4, we discuss the systematic effects considered. Our new best values for  $Y_p$  and the linear regression slope  $dY/dZ$  are presented in §5. The cosmological implications of our new results are discussed in §6. We summarize our conclusions in §7.

## 2. THE SAMPLE

### 2.1. The HeBCD and SDSS subsamples

We determine  $Y_p$  and  $dY/dZ$  independently for two different samples. The HeBCD sample, is composed of 93 different observations of 86 H II regions in 77 galaxies. The majority of these galaxies are low-metallicity BCD galaxies. This sample is essentially the same as the one described in Izotov & Thuan (2004), except that two close pairs of H II regions in the spiral galaxy M101<sup>1</sup> have been added. These four H II regions were observed with the 6.5m MMT on the night of 2004 February 20. Observations were made with the Blue Channel of the MMT spectrograph. We used a  $2'' \times 300''$  slit and a 300 grooves/mm grating in first order. To remove the second-order contamination we use the L-38 blocking filter. The above instrumental set-up gave a spatial scale along the slit of  $0''.6 \text{ pixel}^{-1}$ , a scale perpendicular to the slit of  $1.96 \text{ \AA pixel}^{-1}$ , a spectral range  $3600 - 7500 \text{ \AA}$  and a spectral resolution of  $6 \text{ \AA}$  (FWHM). The Kitt Peak IRS spectroscopic standard star HZ 44 was observed for flux calibration. Spectra of He-Ar comparison arcs were obtained after each observation to calibrate the wavelength scale. The details of data reduction are described in Thuan & Izotov (2005) and they are the same as those for other H II regions from the HeBCD sample. The two-dimensional spectra were bias subtracted and flat-field corrected using IRAF<sup>2</sup>. We then use the IRAF software routines IDENTIFY, REIDENTIFY, FITCOORD, TRANSFORM to perform wavelength calibration and correct for distortion and tilt for each frame. Night sky subtraction was performed using the routine BACKGROUND. The level of night sky emission was determined from the closest regions to the galaxy that are free of galaxian stellar and nebular line emission, as well as of emission from foreground and background sources. One-dimensional spectra were then extracted from each two-dimensional frame using the APALL routine. Before extraction, distinct two-dimensional spectra of the same H II region were carefully aligned using the spatial locations of the brightest part in each spectrum, so that spectra were extracted at the same positions in all subexposures. For all objects, we extracted the brightest part of the H II region. We have summed the individual spectra from each subexposure after manual removal of the cosmic rays hits. The spectra obtained from each subexposure were also checked for cosmic rays hits at the location of strong emission

---

<sup>1</sup> The coordinates of the two H II region pairs are: for the pair M101 No.1 + No.2, R.A.(J2000.0) =  $14^{\text{h}}04^{\text{m}}29^{\text{s}}.5$ , Dec (J2000.0) =  $+54^{\circ}23'47''$  and for the pair M101 No.3 + No.4, R.A.(J2000.0) =  $14^{\text{h}}03^{\text{m}}01^{\text{s}}.2$ , Dec (J2000.0) =  $+54^{\circ}14'29''$ .

<sup>2</sup>IRAF is distributed by National Optical Astronomical Observatory, which is operated by the Association of Universities for Research in Astronomy, Inc., under cooperative agreement with the National Science Foundation.

lines, but none was found.

Particular attention was paid to the derivation of the sensitivity curve. It was obtained by fitting with a high-order polynomial the observed spectral energy distribution of the standard star HZ 44. Because the spectrum of HZ 44 has only a small number of a relatively weak absorption features, its spectral energy distribution is known with good accuracy of  $\lesssim 1\%$  (Oke 1990). Moreover, the response function of the CCD detector is smooth, so we could derive a sensitivity curve with an accuracy better than 1% over the whole optical range.

We show in Tables 1 and 2 (available only in electronic form), the emission line fluxes and the equivalent widths for these H II regions, along with those of the remaining H II regions in the HeBCD sample. They were measured using the IRAF SPLOT routine. The line flux errors listed include statistical errors derived with SPLOT from non-flux calibrated spectra, in addition to errors of 1% of the line fluxes introduced in the standard star absolute flux calibration. The line flux errors will be later propagated into the calculation of abundance errors.

The number of data points (93) is larger than the number of H II regions (86) because several H II regions have independent observations from different telescopes. We treat these independent observations as separate data points in our least-square fitting. In assembling the above sample, we have taken care not to include objects that, for one reason or another, are not appropriate for He abundance determination, as described in Izotov, Thuan & Lipovetsky (1994, 1997) and Izotov & Thuan (1998a,b). In particular, the NW component of I Zw 18 has not been included because its He I  $\lambda 5876$  emission line is strongly affected by the Galactic interstellar Na I  $\lambda 5889, 5895$  absorption line.

The SDSS sample, which we will use as a comparison sample, is composed of 271 low-metallicity H II regions selected from the SDSS DR5. The SDSS (York et al. 2000) offers a gigantic data base of galaxies with well-defined selection criteria and observed in a homogeneous way. In addition, the spectral resolution is much better than that of most previous data bases on emission-line galaxies including all the spectra in the HeBCD sample. It is possible to extract from the SDSS data base a sample of emission-line galaxies with well-defined criteria. Despite the lower quality of its data, this large comparison sample, observed and reduced in a different way, will allow us to check for possible systematic shifts in the linear regressions introduced by different data sets. Its large size will also allow to check for other systematic effects.

The SDSS DR5 provides spectra of some 800 000 galaxies, quasars and stars selected over a sky area of 4783 square degrees, in the wavelength range  $\sim 3800 - 9200\text{\AA}$ , along with tables of measured parameters from these data. From this data base accessible from the

SDSS web page (<http://www.sdss.org/dr5>), we have extracted flux-calibrated spectra of a total of 271 H II regions which satisfy the following selection criteria: 1) the [O III]  $\lambda 4363$  is detected at the level of  $> 2\sigma$  above the noise, allowing a direct heavy element abundance determination by the  $T_e$  method, as was done for the H II regions in the HeBCD sample; 2) the equivalent width of the H $\beta$  emission line  $EW(H\beta)$  is  $\geq 50\text{\AA}$ . This ensures that the effect of underlying He I stellar absorption on the derived He abundances is small; 3) the observed flux of the H $\beta$  emission line  $F(H\beta)$  is  $\geq 10^{-14} \text{ erg s}^{-1} \text{ cm}^{-2}$ . This condition ensures that the SDSS sample contains only bright H II regions with strong emission lines, the fluxes of which can be measured accurately. Since the emission line [O II]  $\lambda 3727$  in the SDSS spectra of galaxies with  $z \lesssim 0.02$  is out of the observed spectral range, we have estimated its flux from the [O II]  $\lambda 7320$ ,  $\lambda 7330$  emission line fluxes. The measurements of the emission line fluxes and the determination of the element abundances were done following the same procedures as for our basic HeBCD sample.

The observed emission line fluxes  $F(\lambda)/F(H\beta)$  and their equivalent widths  $EW(\lambda)$  for all the objects in the two samples are shown respectively in Tables 1 and 2. Because of their large sizes, these tables are available only in electronic form.

## 2.2. Statistical errors

Emission line fluxes of all spectra, in both the HeBCD and SDSS samples, were measured using Gaussian fitting with the IRAF routine SPLLOT. The statistical errors of emission lines in the spectra of the HeBCD sample are calculated using the photon statistics of the lines in the non-flux calibrated spectra. As for the SDSS sample, each spectrum in the SDSS data base is supplemented by a file with the flux error in each pixel which can be used to calculate the errors of the emission lines in each spectra. The mean statistical errors are  $\sim 4\%$  for the brightest He I  $\lambda 5876$  emission line,  $\sim 10\%$  for the He I  $\lambda 4471$  and  $\lambda 6678$  emission lines, and  $\sim 13\%$  for the He I  $\lambda 7065$  emission line, for the combined HeBCD + SDSS sample. As the mean statistical error of the weighted mean He abundance is primarily determined by the statistical error of the intensity of the brightest He I  $\lambda 5876$  emission line, we expect it to be  $\sim 3\text{--}4\%$ , which is the case (see Table 3).

To check the reliability of error determinations for the emission lines in the spectra of our sample, we have considered the flux ratios of the two [O I]  $\lambda 6363$  and [O I]  $\lambda 6300$  lines. These flux ratios are plotted against oxygen abundance in Fig. 1 where objects in the HeBCD sample are shown by filled circles, and those in the SDSS sample by open circles. The solid line shows the mean value of the flux ratio for the combined HeBCD + SDSS sample, and the dashed lines represent  $1\sigma$  dispersions,  $\sim 17\%$  of the mean value. Since the theoretical value



of the [O I]  $\lambda 6363/\lambda 6300$  ratio is constant (its value is  $\sim 1/3$ ) and independent of physical conditions in the H II region, the dispersion of the points around the mean in Fig. 1 gives a good representation of the observational uncertainties. Typically, the flux of [O I]  $\lambda 6300$  is comparable to the flux of He I  $\lambda 4471$  and  $\lambda 6678$  emission lines, with statistical errors of  $\sim 10\%$ . The [O I]  $\lambda 6363$  is  $\sim 3$  times weaker than the [O I]  $\lambda 6300$  line, so its error is  $\sim 17\%$ . This is just the  $1\sigma$  scatter found in Fig. 1 for the [O I] line flux ratio. We conclude that our estimates of the statistical errors for weak emission lines are reliable.

The statistical errors in the emission lines intensities are then propagated in the calculation of errors in electron temperatures, electron number densities and element abundances.

### 3. THE METHOD

#### 3.1. Linear regressions

As in our previous work (see Izotov & Thuan 2004, and references therein), we determine the primordial He mass fraction  $Y_p$  by fitting the data points in the  $Y - O/H$  and  $Y - N/H$  planes with linear regression lines of the form (Peimbert & Torres-Peimbert 1974, 1976; Pagel et al. 1992)

$$Y = Y_p + \frac{dY}{d(O/H)}(O/H), \quad (1)$$

$$Y = Y_p + \frac{dY}{d(N/H)}(N/H), \quad (2)$$

where

$$Y = \frac{4y(1 - Z)}{1 + 4y} \quad (3)$$

is the He mass fraction,  $Z$  is the heavy element mass fraction,  $y = (y^+ + y^{2+}) \times ICF(He^+ + He^{2+})$  is the He abundance,  $y^+ \equiv He^+/H^+$  and  $y^{2+} \equiv He^{2+}/H^+$  are respectively the abundances of singly and doubly ionized He, and  $ICF(He^+ + He^{2+})$  is the ionization correction factor for He. We have assumed  $Z = 18.2(O/H)$  in Eq. 3 which holds for a metallicity  $Z=0.001$  (Maeder 1992).

The assumption of a linear dependence of  $Y$  on  $O/H$  and  $N/H$  appears to be reasonable as there are no evident non-linear trends in the distributions of the data points in the  $Y$  vs  $O/H$  and  $Y$  vs  $N/H$  diagrams (e.g., Izotov & Thuan 2004). The linear regressions (Eqs. 1 and 2) imply that the initial mass function (IMF) averaged stellar yields for different elements do not depend on metallicity. This is the case if the stellar IMF is independent of metallicity. It has been suggested in the past (e.g., Bond et al. 1983) that, at low

metallicities, the IMF may be top-heavy, i.e. there are relatively more massive stars as compared to lower mass stars than at high metallicities. If this is the case, then the IMF-averaged yields would be significantly different for low-metallicity stars as compared to those of more metal-enriched stars, resulting in a non-linear relationship between  $Y$  and  $O/H$  or  $N/H$  (Salvaterra & Ferrara 2003). However, until now, there has not been persuasive evidence for a metallicity dependence of the IMF. Furthermore, the properties of extremely metal-deficient stars remain poorly known, excluding quantitative estimates of possible non-linear effects in the  $Y - O/H$  and  $Y - N/H$  relations. Therefore, in the following analysis, we will continue to use linear regressions (Eqs. 1 and 2) to fit the data.

The slopes of the  $Y - O/H$  and  $Y - N/H$  linear regressions can be written as:

$$\frac{dY}{d(O/H)} = 12 \frac{dY}{dO} = 18.2 \frac{dY}{dZ}, \quad (4)$$

$$\frac{dY}{d(N/H)} = 10.5 \frac{dY}{dN} = 564 \frac{dY}{dZ}, \quad (5)$$

where  $O$ ,  $N$  and  $Z$  are respectively the mass fractions of oxygen, nitrogen and heavy elements. We have assumed that  $O = 0.66Z$  (Maeder 1992) which holds for a metallicity  $Z=0.001$ , an IMF slope  $x=1.35$  (where  $x$  is defined by  $dN/d(\log M) \propto M^x$ ) and  $\log(N/H) - \log(O/H) = -1.55$  (Thuan et al. 1995).

To derive the parameters of the linear regressions, we use the maximum-likelihood method (Press et al. 1992) which takes into account the errors in  $Y$ ,  $O/H$  and  $N/H$  for each object.

### 3.2. $He^+$ emissivities

The derived  $He^+$  abundance  $y^+$  depends on the adopted He I line emissivities. We consider two sets of He I emissivities: the old ones by Benjamin et al. (1999, 2002) which were used by Izotov & Thuan (2004) [Benjamin et al. (2002) take into account both collisional and fluorescent enhancements] and the new ones by Porter et al. (2005) and Bauman et al. (2005), which have been computed using improved radiative and collisional data. Following Izotov, Thuan & Lipovetsky (1994, 1997) and Izotov & Thuan (1998b), we use the five strongest He I  $\lambda 3889$ ,  $\lambda 4471$ ,  $\lambda 5876$ ,  $\lambda 6678$  and  $\lambda 7065$  emission lines to derive  $N_e(He^+)$  and  $\tau(\lambda 3889)$ . Bauman et al. (2005) have estimated the accuracy of new emissivities in the low-density limit and found that accuracy is better than 1% for He I  $\lambda 4471$ ,  $\lambda 5876$ ,  $\lambda 6678$  and  $\lambda 7065$  emission lines, but it is not as good for the He I  $\lambda 3889$  emission line. The He I  $\lambda 3889$  and  $\lambda 7065$  lines play an important role because they are particularly sensitive to both

quantities. Since the He I  $\lambda 3889$  line is blended with the H8  $\lambda 3889$  line, we have subtracted the latter, assuming its intensity to be equal to  $0.107 I(\text{H}\beta)$  (Aller 1984). In our spectra, other He I emission lines are seen, most often He I  $\lambda 3820$ ,  $\lambda 4387$ ,  $\lambda 4026$ ,  $\lambda 4921$ ,  $\lambda 7281$ . However, we do not attempt to use these lines for He abundance determination because they are much weaker as compared to the five brightest lines, and hence have larger uncertainties.

We have used the simple and convenient fits provided by Benjamin et al. (2002) to calculate  $y^+$ s with the Benjamin et al. (1999) emissivities. For the Porter et al. (2005) emissivities, we have assumed the functional dependence of these emissivities on  $N_e$  and  $\tau(\text{He I } \lambda 3889)$ , which results from the collisional and fluorescence enhancements, to be the same as the one for the Benjamin et al. (2002) emissivities. Eqs. 6 – 10 give the linear fits we have adopted for the ratios of the two sets of emissivities in the temperature range  $T_e = 10^4 - 2 \times 10^4$  and an electron number density  $N_e = 100 \text{ cm}^{-3}$ , for each of the five lines:

$$y_P^+(\lambda 3889) = y_B^+(\lambda 3889)/(1.079 - 0.052 \times t), \quad (6)$$

$$y_P^+(\lambda 4471) = y_B^+(\lambda 4471)/(1.020 - 0.026 \times t), \quad (7)$$

$$y_P^+(\lambda 5876) = y_B^+(\lambda 5876)/(0.956 + 0.011 \times t), \quad (8)$$

$$y_P^+(\lambda 6678) = y_B^+(\lambda 6678)/(0.938 + 0.028 \times t), \quad (9)$$

$$y_P^+(\lambda 7065) = y_B^+(\lambda 7065)/(1.051 - 0.040 \times t), \quad (10)$$

where  $y_B^+$  and  $y_P^+$  are respectively  $\text{He}^+$  abundances calculated with Benjamin et al. (1999) (B) and Porter et al. (2005) (P) emissivities and  $t = 10^{-4} T_e$ . We found that, with Porter et al. (2005) emissivities,  $\text{He}^+$  abundances are higher than those derived with Benjamin et al. (1999) emissivities by about 0 – 2 percent for the  $\lambda 4471$  line, and by about 5 – 6 percent for the  $\lambda 5876$  line, in the range  $t = 1 - 2$ .

### 3.3. A Monte Carlo algorithm for determining the best value of $y^+$

In addition to the emissivities, the derived  $y^+$  abundances depend also on a number of other parameters: the fraction  $\Delta I(\text{H}\alpha)/I(\text{H}\alpha)$  of the  $\text{H}\alpha$  emission line flux due to collisional excitation, the electron number density  $N_e(\text{He}^+)$ , the electron temperature  $T_e(\text{He}^+)$ , the equivalent widths  $\text{EW}_{abs}(\lambda 3889)$ ,  $\text{EW}_{abs}(\lambda 4471)$ ,  $\text{EW}_{abs}(\lambda 5876)$ ,  $\text{EW}_{abs}(\lambda 6678)$  and  $\text{EW}_{abs}(\lambda 7065)$  of He I stellar absorption lines, and the optical depth  $\tau(\lambda 3889)$  of the He I  $\lambda 3889$  emission line. To determine the best value of  $y_{wm}^+$  (defined in Eq. 12), we use the Monte Carlo procedure described in Izotov & Thuan (2004), randomly varying each of the above parameters within a specified range. First, we take into account collisional excitation effects for hydrogen. The value of the fraction of the  $\text{H}\alpha$  flux due to collisional excitation

is randomly generated 100 times within an adopted range. The fraction of the  $H\beta$  emission line flux due to the collisional excitation is adopted to be three times less than that of the  $H\alpha$  flux. For each generated fraction, the fluxes of the  $H\alpha$  and  $H\beta$  lines due to the collisional excitation are subtracted from the total observed fluxes and then all emission line fluxes are corrected for interstellar extinction and element abundances are calculated.

To calculate  $y^+$  we vary simultaneously and randomly  $N_e(\text{He}^+)$ ,  $T_e(\text{He}^+)$  and  $\tau(\lambda 3889)$  within their respective adopted ranges. We make a total of  $10^5$  such realizations for every H II region, for a given fraction of the  $H\alpha$  emission line flux due to collisional excitation. Thus, the total number of Monte Carlo realizations we have performed for each H II region is  $100 \times 10^5 = 10^7$ . As for the He I underlying stellar absorption, we assume fixed values for  $\text{EW}_{abs}(\lambda 4471)$ , chosen to be between 0 and  $0.5\text{\AA}$ , and for the  $\text{EW}_{abs}(\lambda 3889)/\text{EW}_{abs}(\lambda 4471)$ ,  $\text{EW}_{abs}(\lambda 5876)/\text{EW}_{abs}(\lambda 4471)$ ,  $\text{EW}_{abs}(\lambda 6678)/\text{EW}_{abs}(\lambda 4471)$ , and  $\text{EW}_{abs}(\lambda 7065)/\text{EW}_{abs}(\lambda 4471)$  ratios.

For each H II region, we find the best solution for  $y_{wm}^+$  in the multi-parameter space defined above by minimizing the quantity

$$\chi^2 = \sum_i^n \frac{(y_i^+ - y_{wm}^+)^2}{\sigma^2(y_i^+)}, \quad (11)$$

where  $y_i^+$  is the  $\text{He}^+$  abundance derived from the flux of the He I emission line labeled  $i$ , and  $\sigma(y_i^+)$  is the statistical error of  $y_i^+$ . The quantity  $y_{wm}^+$  is the weighted mean of the  $\text{He}^+$  abundance as given by the equation

$$y_{wm}^+ = \frac{\sum_i^k y_i^+ / \sigma^2(y_i^+)}{\sum_i^k 1 / \sigma^2(y_i^+)}. \quad (12)$$

We use all five He I emission lines to calculate  $\chi^2$  (i.e.,  $n = 5$ ), but only three lines, He I  $\lambda 4471$ ,  $\lambda 5876$  and  $\lambda 6678$  to compute  $y_{wm}^+$  ( $k = 3$ ). This is because the fluxes of He I  $\lambda 3889$  and  $\lambda 7065$  emission lines are more uncertain as compared to the other three He I emission lines.

An estimate of the  $1\sigma_{\text{sys}}$  systematic error of  $y_{wm}^+$  can be obtained from  $\Delta\chi^2$ . This quantity depends on the number of degrees of freedom in the problem which is the difference between the number of observational constraints, equal to 5 (the five He I emission line fluxes), and the number of the free parameters, equal to 4 [the fraction  $\Delta I(H\alpha)/I(H\alpha)$  due to collisional excitation of the  $H\alpha$  emission line,  $T_e(\text{He}^+)$ ,  $N_e(\text{He}^+)$  and  $\tau(\lambda 3889)$ ]. Since the number of degrees of freedom is  $5 - 4 = 1$ , then  $\Delta\chi^2 = 1$  (Press et al. 1992). Thus the systematic error  $\sigma_{\text{sys}}$  is the  $1\sigma$  dispersion of the computed values of  $y_{wm}^+$  for solutions with  $\chi^2$  between  $\chi_{\text{min}}^2$  and  $\chi_{\text{min}}^2 + 1$ . The total error for  $y_{wm}^+$  is then given by  $\sigma_{\text{tot}}^2 = \sigma_{\text{stat}}^2 + \sigma_{\text{sys}}^2$ .

Additionally, in those cases when the nebular He II  $\lambda 4686$  emission line was detected, we have added the abundance of doubly ionized helium  $y^{2+} \equiv \text{He}^{2+}/\text{H}^+$  to  $y^+$ . Although the  $\text{He}^{2+}$  zone is hotter than the  $\text{He}^+$  zone, we have adopted  $T_e(\text{He}^{2+}) = T_e(\text{He}^+)$ . The last assumption has only a minor effect on the  $y$  value, because  $y^{2+}$  is small ( $\leq 3\%$  of  $y^+$ ) in all cases.

### 3.4. A basic set of parameters for Monte Carlo calculations

In order to study the dependence of  $Y_p$  on the various parameters characterizing different systematic effects, we define a reference set of parameters which we will call the “basic set”. We wish to see how, by changing different parameters, the  $y$  values change, as compared to those corresponding to the basic set. The basic set of parameters is defined in the following way : 1) the electron temperature of the  $\text{He}^+$  zone is varied in the range  $T_e(\text{He}^+) = (0.95 - 1.0) \times T_e(\text{O III})$ ; 2) oxygen and nitrogen abundances are calculated adopting an electron temperature equal to  $T_e(\text{O III})$ ; 3)  $N_e(\text{He}^+)$  and  $\tau(\lambda 3889)$  vary respectively in the ranges  $10 - 450 \text{ cm}^{-3}$  and  $0 - 5$ ; 4) the fraction of  $\text{H}\alpha$  emission due to collisional excitation is varied in the range  $0\% - 5\%$ ; 5) the equivalent width of the He I  $\lambda 4471$  absorption line is fixed to  $\text{EW}_{abs}(\lambda 4471) = 0.4 \text{ \AA}$ ; 6) the equivalent widths of the other absorption lines are fixed according to the ratios  $\text{EW}_{abs}(\lambda 3889)/\text{EW}_{abs}(\lambda 4471) = 1.0$ ,  $\text{EW}_{abs}(\lambda 5876)/\text{EW}_{abs}(\lambda 4471) = 0.3$ ,  $\text{EW}_{abs}(\lambda 6678)/\text{EW}_{abs}(\lambda 4471) = 0.1$  and  $\text{EW}_{abs}(\lambda 7065)/\text{EW}_{abs}(\lambda 4471) = 0.1$ . The justification of the values of these ratios is given in Izotov & Thuan (2004) and in §4.4. The ionization correction factor  $ICF(\text{He}^+ + \text{He}^{2+})$  is discussed in §4.6.

## 4. SYSTEMATIC EFFECTS

We will consider successively the following systematic effects in the derivation of He abundances: 1) He I emissivities; 2) reddening; 3) the temperature structure of the H II region, i.e. the temperature difference between  $T_e(\text{He}^+)$  and  $T_e(\text{O III})$ ; 4) underlying stellar He I absorption; 5) collisional excitation of hydrogen lines; 6) the ionization structure of the H II region; and 7) the deviation of hydrogen and He I recombination line fluxes from case B. At the very end, we will also consider possible biases introduced by different samples not observed and reduced in the same way by deriving  $Y_p$  independently for the HeBCD and SDSS samples and comparing the results. However, we will not discuss here collisional and fluorescent enhancements of the He I emission lines. These were discussed in detail by e.g. Benjamin et al. (1999, 2002). We only note that the importance of these two effects depends on the specific He I emission line considered. In particular, the correction for

collisional excitation of the He I  $\lambda 5876$  emission line can decrease its flux by as much as  $\sim 17\%$ , depending on  $T_e(\text{He}^+)$  and  $N_e(\text{He}^+)$ . In the following, we apply the corrections for collisional and fluorescent enhancements, adopting the most recent analytical fits of Benjamin et al. (1999, 2002).

Effects 1 – 6 have been considered in many previous papers on the determination of the primordial He abundance. However, previous analyses were typically based on small samples and/or not all systematic effects were considered. By contrast, the present study has two major advantages: 1) it is based on the largest sample of H II regions ever assembled for the determination of  $Y_p$ ; and 2) all important known systematic effects are taken into account using a Monte-Carlo approach.

#### 4.1. He I emissivities

First, we consider the difference in the primordial He mass fraction  $Y_p$  caused by using two different sets of He I line emissivities. We adopt the basic set of parameters from §3.4 except for: a) the range of  $T_e(\text{He}^+)$  variations, which we adopt here to be  $(0.9 - 1.0) \times T_e(\text{O III})$ , the same as that used by Izotov & Thuan (2004), and b) the oxygen and nitrogen abundances which are calculated with the electron temperature set to  $T_e(\text{He}^+)$ . There are two differences between the procedures of Izotov & Thuan (2004) and the ones used here: 1) the average  $y^+$  is calculated using only three He I emission lines while the computation of  $\chi^2$  takes into account all five lines. Izotov & Thuan (2004) included all five lines for the calculation of both  $y^+$  and  $\chi^2$ ; 2) Izotov & Thuan (2004) adopted  $\text{EW}_{abs}(\text{H7} + \lambda 3889) = 3.0 \text{ \AA}$  instead of the relation  $\text{EW}_{abs}(\lambda 3889) = \text{EW}_{abs}(\lambda 4471)$  adopted here. However, we will show later in this section that the variations of the  $\text{EW}_{abs}(\lambda 3889)$  have little effect on the derived  $Y_p$ .

In Fig. 2a and 2b we show the linear regressions  $Y - \text{O/H}$  and  $Y - \text{N/H}$  for the HeBCD sample where the values of  $Y$  are calculated with the Benjamin et al. (2002) He I emissivities. From these regressions we derive  $Y_p = 0.2440 \pm 0.0013$  and  $0.2464 \pm 0.0010$ . If  $\text{EW}_{abs}(\text{H7} + \lambda 3889)$  is set to  $3.0 \text{ \AA}$  instead of adopting the relation  $\text{EW}(\lambda 3889) = \text{EW}(\lambda 4471)$ , then  $Y_p = 0.2435 \pm 0.0013$  and  $0.2462 \pm 0.0010$  respectively for the  $Y - \text{O/H}$  and  $Y - \text{N/H}$  regressions. These values are in agreement with  $Y_p = 0.2421 \pm 0.0020$  and  $0.2446 \pm 0.0016$  obtained by Izotov & Thuan (2004) for their sample of 7 H II regions. Note that the value of  $Y_p$  derived from the  $Y - \text{N/H}$  regression is always slightly greater than the one derived from the  $Y - \text{O/H}$  regression. This is because the N/O abundance ratio tends to increase with increasing oxygen abundance (e.g. Izotov & Thuan 1999; Izotov et al. 2006).

Figs. 2c and 2d show the linear regressions  $Y - \text{O}/\text{H}$  and  $Y - \text{N}/\text{H}$  when the Porter et al. (2005) He I emissivities are used. We obtain  $Y_p = 0.2482 \pm 0.0012$  and  $0.2507 \pm 0.0009$  from these regressions. It is seen that the use of the new emissivities increases  $Y_p$  by  $\sim 1.7\%$ .

In the analysis of the other systematic effects, we will consider mainly helium abundances obtained with the Porter et al. (2005) emissivities, with only occasional mention of helium abundances obtained with the Benjamin et al. (2002) emissivities for comparison.

## 4.2. Reddening

Izotov, Thuan & Lipovetsky (1994, 1997) and Izotov & Thuan (1998a, 2004) have used the Whitford (1958) reddening curve with  $R_V = A_V/E(B - V) = 3.2$  to correct the line intensities for extinction. The derived value of  $Y_p$  should not be very sensitive to the choice of a particular reddening curve because of the way the extinction correction is applied: the fluxes of the Balmer lines are corrected for extinction so that the resulting flux ratios correspond to the theoretical values, independently of the adopted reddening law. Then, the corrected fluxes of the other emission lines are not sensitive to the particular reddening law as well.

To check the sensitivity of  $Y_p$  on the adopted reddening law, we have also considered the Cardelli et al. (1989) reddening curves with  $R_V = 2.5, 3.2$  and  $4.0$ . We find that the  $Y_p$  derived with the Cardelli et al. (1989) reddening curve and  $R_V = 3.2$  is only  $\sim 0.3\%$  higher than the value derived with the Whitford (1958) reddening curve. The  $Y_p$  derived with  $R_V = 2.5$  is  $\sim 0.4\%$  lower than the one with  $R_V = 3.2$ , while the  $Y_p$  derived with  $R_V = 4.0$  is  $\sim 0.2\%$  higher. The effect of various reddening laws on the derived  $Y_p$  is indeed small. Therefore, for consistency with our previous work, we have adopted the Whitford (1958) reddening law with  $R_V = 3.2$ , the same as the one used by Izotov, Thuan & Lipovetsky (1994, 1997) and Izotov & Thuan (1998a, 2004).

## 4.3. Temperature structure

To derive the He abundances, Izotov, Thuan & Lipovetsky (1994, 1997) and Izotov & Thuan (1998b) have assumed that the temperatures  $T_e(\text{He}^+)$  and  $T_e(\text{O III})$ , averaged over the whole H II region, are equal.  $T_e(\text{O III})$  is determined from the observed  $[\text{O III}]\lambda 4363/(\lambda 4959 + \lambda 5007)$  emission line flux ratio. However, because of the high sensitivity of the flux of the auroral  $[\text{O III}]\lambda 4363$  emission line to temperature,  $T_e(\text{O III})$  tends to be characteristic of the hotter zones in the H II region, and may be expected to be higher than  $T_e(\text{He}^+)$ . On the

other hand,  $T_e(\text{H}^+)$  and  $T_e(\text{He}^+)$  are derived from the recombination spectrum of ionized hydrogen and helium, which is not very sensitive to temperature. Therefore, the assumption  $T_e(\text{He}^+) = T_e(\text{H}^+)$ , which we adopt here, seems reasonable, the  $\text{H}^+$  and  $\text{He}^+$  zones in high-excitation H II regions being nearly coincident.

To account for the difference between  $T_e(\text{O III})$  and  $T_e(\text{He}^+)$ , Peimbert (1967) has developed a formalism based on the average temperature  $T_0$  and the mean square temperature variation  $t^2$  in an H II region. Then  $T_e(\text{He}^+)$  and  $T_e(\text{O III})$  can be expressed as functions of  $T_0$  and  $t^2$ , with  $T_e(\text{O III}) \geq T_e(\text{He}^+)$ . This approach has been applied by Peimbert et al. (2002) for the determination of the He abundance in several low-metallicity dwarf galaxies. They find that the difference between  $T_e(\text{O III})$  and  $T_e(\text{He}^+)$  results in a reduction of the He mass fraction by 2 – 3 percent as compared to the case with  $T_e(\text{O III}) = T_e(\text{He}^+)$ .

Until very recently, no direct measurement of  $T_e(\text{H}^+)$  has been carried out for extremely metal-deficient H II regions, those which carry the most weight in the determination of  $Y_p$ . All existing measurements of  $T_e(\text{H}^+)$  based on the Balmer jump or the Paschen jump, have been done for relatively metal-rich H II regions. The lowest-metallicity H II region for which such a measurement was performed is Mrk 71 with  $12 + \log \text{O}/\text{H} \sim 7.9$  (Gonzalez-Delgado et al. 1994),  $\sim 5 - 6$  times more metal-rich as compared to the lowest-metallicity H II regions in our sample. Other measurements of  $T_e(\text{H}^+)$  have been done for 30 Dor in the Large Magellanic Cloud ( $12 + \log \text{O}/\text{H} = 8.3$ , Peimbert 2003) and some nearly solar-metallicity H II regions in our Galaxy (Peimbert et al. 1993, 2000; Esteban et al. 1998; Garcia-Rojas et al. 2004, 2005).

Using the Balmer and Paschen jumps, Guseva et al. (2006) have measured  $T_e(\text{H}^+)$  for an extensive sample of 47 H II regions which includes the most metal-deficient BCDs known, such as SBS 0335–052W, I Zw 18 and SBS 0335–052E. Contrary to the suggestions of Peimbert (1967) and Peimbert et al. (2002), they found no statistically significant difference between  $T_e(\text{O III})$  and  $T_e(\text{H}^+)$ , but could not exclude small differences of  $\lesssim 5\%$ .

To investigate the effect of these possible small differences between  $T_e(\text{O III})$  and  $T_e(\text{He}^+) = T_e(\text{H}^+)$  on  $Y_p$ , we have derived  $Y - \text{O}/\text{H}$  regression fits for the two sets of He I emissivities, both for the case where  $T_e(\text{He}^+)$  is varied in the range  $(0.95 - 1.0) \times T_e(\text{O III})$  (Fig. 3a), and for the one where  $T_e(\text{He}^+) = T_e(\text{O III})$  (Fig. 3h). All other parameters are those from the basic set. Comparison of Fig. 3a (the one corresponding to the basic set of parameters) and Fig. 3h shows that assuming  $T_e(\text{He}^+) = T_e(\text{O III})$  instead of varying it in the range  $(0.95 - 1.0) \times T_e(\text{O III})$  gives a  $Y_p$  larger by about  $\sim 1.0\%$ . We note that if  $T_e(\text{He}^+)$  is different from  $T_e(\text{O III})$ , it may also be used for the determination of  $\text{O}/\text{H}$  (Fig. 3i). If we do so, then  $Y_p$  is increased by only  $\lesssim 0.3\%$  compared to the basic regression in Fig. 3a, but the slope of the regression line is significantly shallower as compared to the case where oxygen abundance



is calculated with  $T_e(\text{O III})$ . This is because the oxygen abundance derived with  $T_e(\text{He}^+)$  is larger than the one derived with  $T_e(\text{O III})$ , and  $\Delta(\text{O}/\text{H}) = \text{O}/\text{H}[T_e(\text{He}^+)] - \text{O}/\text{H}[T_e(\text{O III})]$  is larger for high-metallicity H II regions than for low-metallicity ones.

We have also considered the changes on  $Y_p$  if we adopt the temperature variations of  $T_e(\text{He}^+)$  proposed by Peimbert et al. (2002). Their Fig. 1 shows that  $T_e(\text{He}^+)$  varies within a range  $(0.97 - 1) \times T_e(\text{O III})$  for H II regions with  $T_e(\text{O III}) = 20000\text{K}$ , with the mean square temperature variation  $t^2$  ranging between 0 and 0.04, but increases to  $(0.88 - 1) \times T_e(\text{O III})$  for H II regions with  $T_e(\text{O III}) = 10000\text{K}$ , for the same range of  $t^2$ . By adopting the above temperature dependence of  $T_e(\text{He}^+)$ , we obtain  $Y_p = 0.2506$ , essentially the same value as the one obtained from the basic regression.

#### 4.4. Underlying stellar He I absorption

It has long been recognized (Rayo et al. 1982; Kunth & Sargent 1983; Dinerstein & Shields 1986; Pagel et al. 1992; Olofsson 1995) that absorption caused by hot stars in the He I lines can induce an underestimation of the intensities of the nebular He I lines. In particular, Izotov & Thuan (1998a) have shown that the neglect of He I underlying stellar absorption has led to the derivation of a very low helium mass fraction in I Zw 18, the second most metal-deficient BCD known (Pagel et al. 1992; Olive et al. 1997). Recently, Izotov & Thuan (2004), Olive & Skillman (2004) and Fukugita & Kawasaki (2006) have taken into account this effect to derive  $Y_p$ , using a subsample of the HeBCD sample of Izotov & Thuan (2004).

González Delgado et al. (1999) have calculated synthetic spectra of H Balmer and He I absorption lines in starburst and poststarburst galaxies. They predict the equivalent width of the He I  $\lambda 4471$  absorption line to be in the range  $\sim 0.4 - 0.5 \text{ \AA}$ , or  $\lesssim 10\%$  of the He I  $\lambda 4471$  emission line equivalent width for young starbursts with an age  $\lesssim 5 \text{ Myr}$ , which is the case for the H II regions in our sample.

Unfortunately, those authors did not calculate absorption line equivalent widths for the other prominent He I lines. We expect however that the effect of underlying absorption is smaller for the He I  $\lambda 5876$ ,  $\lambda 6678$  and  $\lambda 7065$  emission lines. This, for the following reason. It is known that the equivalent widths are not the same for all hydrogen absorption lines. For a fixed age of the stellar population,  $\text{EW}_{abs}$  is the largest for  $\text{H}\delta$ , then decreases progressively for  $\text{H}\gamma$ ,  $\text{H}\beta$  and  $\text{H}\alpha$  at longer wavelengths. A similar trend is likely to hold for He I absorption lines: the longer the wavelength of the line, the smaller its  $\text{EW}_{abs}$ . It is not clear, however, how strong is underlying absorption for the He I  $\lambda 3889$  line, at the short wavelength end. In

any case, underlying stellar absorption must be taken into account for all He I lines if we are to achieve the desired high accuracy of  $\lesssim 1\%$  in the primordial He abundance determination.

Among the five He I emission lines used here, the effect of the underlying stellar absorption is most important for the blue He I  $\lambda 4471$  emission line because it has the lowest equivalent width. For the redder lines, especially for the He I  $\lambda 5876$  emission line which carries the highest weight in the  $Y$  determination, the effect of underlying stellar absorption is likely considerably lower. As for the blue He I  $\lambda 3889$  emission line, its flux is  $\gtrsim 2$  times greater than that of the He I  $\lambda 4471$  emission line and hence the effect of the underlying stellar absorption is also expected to be lower. However, the situation with this line is more complicated compared to other lines because of its blending with the hydrogen emission line H7.

We have presented our choice for the various ratios linking the absorption equivalent width of the He I  $\lambda 4471$  line to those of the other He I lines in our discussion of the basic set of parameters. While the choice of those ratios may appear arbitrary and is somewhat subjective since, with the exception of the  $\lambda 4471$  line, we do not have any guidance from observations or models concerning the equivalent widths of the He I absorption lines, we can estimate the effect of different adopted  $EW_{abs}$  on  $Y_p$ . Thus, assuming larger  $EW_{abs}$  for the He I  $\lambda 5876$ ,  $\lambda 6678$  and  $\lambda 7065$  lines, in the range 0.5 – 1.0 that of the  $\lambda 4471$  line, would result in a value of  $Y_p$  that can be as much as  $\sim 1\%$  larger than the basic value. However, our calculations show that for the majority of the H II regions, the  $\chi^2_{min}$  values obtained with the larger  $EW_{abs}$  for the  $\lambda 5876$ ,  $\lambda 6678$  and  $\lambda 7065$  lines are  $\sim 2$  times larger than the  $\chi^2_{min}$  value obtained with the basic parameter set. Additionally, the dispersion of the points in the  $Y - O/H$  and  $Y - N/H$  diagrams is higher. We also made calculations with the case  $EW_{abs}(\lambda 5876) = 0.1 \times EW_{abs}(\lambda 4471)$ . The resulting  $Y_p$  is only  $\lesssim 0.3\%$  lower than the basic one. In summary, variations of  $EW_{abs}$  for He I lines other than  $\lambda 4471$  do not affect much  $Y_p$ . Therefore, we will adopt the basic  $EW_{abs}$  ratios in our  $Y_p$  determination.

Once the  $EW_{abs}$  ratios chosen, we need to fix the absorption equivalent width of the  $\lambda 4471$  line. To check the influence of the correction of He I emission line fluxes for underlying stellar absorption on  $Y_p$ , we consider two cases: case a) where there is no underlying absorption, i.e.  $EW_{abs}(\lambda 4471) = 0$  and case b) where  $EW_{abs}(\lambda 4471) = 0.5 \text{ \AA}$ , the maximal equivalent width expected for underlying absorption. In Fig. 3b and 3c, we show the linear regressions respectively for cases (a) and (b). It is seen that the difference in  $Y_p$  between the two cases is  $\sim 3\%$ . In addition, we have also checked how variations of  $EW_{abs}(\lambda 3889)$  affect  $Y_p$ . Since the He I  $\lambda 3889$  emission line is blended with the hydrogen H7 emission line, we have considered, in addition to the basic case shown in Fig. 3a where  $EW_{abs}(\lambda 3889) = EW_{abs}(\lambda 4471)$ , also the case where  $EW_{abs}(H7 + \lambda 3889) = 3.0 \text{ \AA}$ , shown in Fig. 3d. The second case gives a  $Y_p$

which is  $\sim 1.0\%$  lower than the value given by the basic model. However, it has a  $\chi^2_{min}$  which is significantly larger than the one of the basic model.

The effect of underlying stellar absorption is greater in H II regions with lower equivalent widths of He I emission lines. This allows us to check whether the value of  $0.4\text{\AA}$  which we have adopted for  $EW_{abs}(\lambda 4471)$  in the basic set is reasonable or not. If the adopted value is not correct, then the values of  $Y_p$  derived from H II regions with lower  $EW(H\beta)$ s and higher  $EW(H\beta)$ s will be different, as the first ones will give underestimated He abundances as compared to the latter ones. In Figs. 3e and 3f, we show respectively the linear regressions for the subsamples of H II regions with  $EW(H\beta) > 100\text{\AA}$  and of those with  $EW(H\beta) > 200\text{\AA}$ . It is seen that the  $Y_p$  derived for the HeBCD subsample with  $EW(H\beta) > 100\text{\AA}$  (Fig. 3e) is only slightly ( $\lesssim 0.2\%$ ) lower than the value derived for the HeBCD subsample with  $EW(H\beta) > 200\text{\AA}$  (Fig. 3f). This shows that  $EW_{abs}(\text{He I } \lambda 4471) = 0.4\text{\AA}$  and the ratios of  $EW_{abs}$  adopted in the basic model characterize well the underlying He I stellar absorption.

Probably, as proposed by Porter et al. (2006), the best check of the appropriateness of the basic set of  $EW_{abs}$ s comes from comparing the abundance of singly ionized He  $y^+$ , calculated separately for each of the three He I  $\lambda 4471$ ,  $\lambda 5876$  and  $\lambda 6678$  emission lines, with their weighted mean  $y^+_{wm}$ . We show in Fig. 4a the dependence of  $(y^+ - y^+_{wm})$  on the He I emission line equivalent width  $EW_{em}$ , for each of the three emission lines, in the case where underlying absorption is not taken into account. It is seen that there are no significant offsets between the  $y^+$ s derived from the He I  $\lambda 5876$  and  $\lambda 6678$  emission lines (labeled respectively by stars and open circles), suggesting that the effect of underlying absorption for those lines is relatively small. On the other hand, the  $y^+$ s derived from the He I  $\lambda 4471$  emission line (filled circles) are systematically lower than those derived from the other two emission lines, suggesting that underlying stellar absorption is significant. Figs. 4b - 4d show the same dependences as in Fig. 4a, but for successively increasing values of  $EW_{abs}(\lambda 4471)$ , varying from  $0.2\text{\AA}$  to  $0.5\text{\AA}$ . For the other He I lines we adopt the same ratios of  $EW_{abs}$  to  $EW_{abs}(\lambda 4471)$  as those in the basic model. It is seen from Figs. 4c that the  $y^+$ s derived for He I  $\lambda 4471$  with  $EW_{abs}(\lambda 4471) = 0.4\text{\AA}$  are in good agreement with the ones for the other two lines. However, the  $y^+(\lambda 4471)$  derived with lower and higher  $EW_{abs}(\lambda 4471)$ s are respectively lower and higher than the  $y^+$  values derived for the He I  $\lambda 5876$  and  $\lambda 6678$  lines (compare Fig. 4b with Fig. 4d). Porter et al. (2006) have also suggested to use a simple mean  $y^+_m$  instead of the weighted mean  $y^+_{wm}$  used in our analysis. In Figs. 5a and 5b we show the dependence of  $(y^+ - y^+_m)$  on  $EW_{em}$  for two choices of  $EW_{abs}(\lambda 4471)$ : 0 (Fig. 5a) and  $0.4\text{\AA}$  (Fig. 5b). Similarly to Fig. 4a, there is a clear difference between the  $y^+$  derived from the He I  $\lambda 4471$  line and those derived from the other two He I lines when underlying stellar absorption is not taken into account (Fig. 5a). On the other hand, there is no clear offset in the  $y^+$  derived from the different He I lines in Fig. 5b, where  $EW_{abs}(\lambda 4471) = 0.4\text{\AA}$ . The

primordial He abundance  $Y_p$  derived from the  $Y - O/H$  regression, using a simple mean for  $y^+$  and  $EW_{abs}(\lambda 4471) = 0$  (Fig. 5c) is  $\sim 0.8\%$  lower than the  $Y_p$  obtained using a weighted mean for  $y^+$  (Fig. 3b). This is because the He I  $\lambda 4471$  line contributes more to the simple mean than to the weighted mean. On the other hand, no difference in  $Y_p$  is found when  $EW_{abs}(\lambda 4471)$  is set to  $0.4\text{\AA}$ , irrespective of whether  $y^+$  is computed with a weighted mean or a simple mean (compare Figs. 5d and 3a).

All the above considerations lead us to conclude that the basic set of  $EW_{abs}$ s adopted for the He I lines is the most appropriate one to use.

#### 4.5. Collisional excitation of the H lines

It has generally been assumed in abundance studies that deviations of the observed  $H\alpha/H\beta$  flux ratio from the theoretical recombination value are entirely due to interstellar extinction. Davidson & Kinman (1985) first noted that in the hot and dense H II regions of BCDs, collisional excitation of hydrogen emission lines can be important and affect the derived He/H ratio. Stasińska & Izotov (2001) estimated that this effect can result in an upward correction in the He abundances of up to 5%, assuming that the excess of the  $H\alpha/H\beta$  flux ratio above the theoretical recombination value is due only to collisional excitation. However, new computations of the effective collision strength for excitation of hydrogen (Anderson et al. 2002) give a smaller enhancement of the Balmer lines due to collisional excitation. Luridiana et al. (2003) have performed a very detailed analysis of 3 H II regions, including a tailored photoionization analysis and a discussion of reddening. They find that the collisional contribution to  $H\alpha$  in those objects may reach 8 % and that to  $H\beta$  2 – 2.5 %. Thus, in our Monte Carlo approach, we have varied the fraction of the  $H\alpha$  emission line flux due to collisional excitation,  $\Delta I(H\alpha)/I(H\alpha)$ , in the range 0 – 5%. Its value is derived together with other parameters by the minimization of  $\chi^2$  as defined in Eq. 11. To check how the inclusion of hydrogen collisional excitation influences  $Y_p$ , we have also calculated the linear regression for the case where that effect is not taken into account, i.e.  $\Delta I(H\alpha) = 0$ . The result is shown in Fig. 3k. Comparison with the basic regression (Fig. 3a) shows that ignoring hydrogen collisional excitation results in a decrease of  $Y_p$  by  $\sim 1.2\%$ .<sup>3</sup>

---

<sup>3</sup>In the above analysis, we have adopted a ratio of  $H\alpha$  to  $H\beta$  emissivities due to collisional excitation equal to 3. The referee has pointed out that this ratio may be higher. We have estimated it to be 5 – 7 in the temperature range  $T_e = 10000\text{K} - 20000\text{K}$ , consistent with the Anderson et al. (2002) determination. The consequence of adopting a ratio of  $H\alpha$  to  $H\beta$  emissivities due to collisional excitation equal to 5 would be to increase  $Y_p$  by only 0.3%, using the HeBCD sample and in the case of the basic model.

#### 4.6. Ionization structure

Another source of systematic uncertainty comes from the assumption that the  $\text{H}^+$  and  $\text{He}^+$  zones in the H II region are spatially coincident. However, depending on the hardness of the ionizing radiation, the radius of the  $\text{He}^+$  zone can be smaller than the radius of the  $\text{H}^+$  zone in the case of soft ionizing radiation, or larger in the case of hard radiation. In the former case, a correction for unseen neutral helium should be made, resulting in an ionization correction factor  $ICF(\text{He}^+ + \text{He}^{2+}) > 1$  and hence a higher helium abundance. In the latter case, the situation is opposite and  $ICF(\text{He}^+ + \text{He}^{2+}) < 1$ . The ionization correction factor problem has been discussed in several studies (Stasińska 1980; Pagel et al. 1992; Steigman et al. 1997; Olive et al. 1997; Viegas et al. 2000; Peimbert et al. 2000; Ballantyne et al. 2000; Sauer & Jedamzik 2002). It was concluded that the correction of the helium abundance can be as high as several percent in either downward or upward directions, depending on the hardness of the radiation and the ionization parameter  $U$ . Sauer & Jedamzik (2002) have calculated an extensive grid of photoionized H II region models which give correction factors as functions of hardness and  $U$ . Their conclusion was that a downward correction of  $Y$  by as much as 6% and 2% is required respectively for ionization parameters  $\log U = -3.0$  and  $-2.5$ . However, if  $\log U \gtrsim -2.0$ , which is the case for the majority of our H II regions, the downward correction is  $\lesssim 1\%$ .

Ballantyne et al. (2000) have suggested that  $ICF(\text{He}^+ + \text{He}^{2+})$  can be estimated from the  $[\text{O III}]\lambda 5007/[\text{O I}]\lambda 6300$  emission line flux ratio. They have calculated an extensive grid of photoionized H II region models, spanning a wide range of metallicity and excitation and with different models for the ionizing stellar radiation. Ballantyne et al. (2000) have concluded that the  $ICF$  can be significantly lower than unity in hot H II regions. However, if a H II region has a  $[\text{O III}]\lambda 5007/[\text{O I}]\lambda 6300$  ratio greater than 300, then their models show that, regardless of its metallicity, it will have an  $ICF$  very close to unity. Using the observations of Izotov & Thuan (1998b), Ballantyne et al. (2000) have found that the scatter of the data points for H II regions with  $[\text{O III}]\lambda 5007/[\text{O I}]\lambda 6300 > 300$  in the  $Y - \text{O}/\text{H}$  diagram is some 20% smaller than that for the whole sample, and have derived  $Y_p = 0.2489 \pm 0.0030$  for the restricted sample. However, their analysis suffers from the small number of H II regions in the restricted sample. In particular, they found a negative  $dY/d(\text{O}/\text{H})$  slope, which leads to a high value of  $Y_p$ . Such a negative slope is unphysical and cannot be justified by any chemical evolution model, with any star formation scenario.

To check how the  $ICF$  is related to the  $[\text{O III}]\lambda 5007/[\text{O I}]\lambda 6300$  ratio, we show in Fig. 6  $Y - \text{O}/\text{H}$  regression lines for the combined HeBCD + SDSS sample, with different cutoffs of the  $[\text{O III}]\lambda 5007/[\text{O I}]\lambda 6300$  ratio. The HeBCD H II regions are shown by filled circles and the SDSS H II regions by open circles. We adopt  $ICF(\text{He}^+ + \text{He}^{2+}) = 1$  for all H II

regions. All other parameters are those of the basic set (§3.4). It is seen that the scatter in the  $Y - \text{O}/\text{H}$  diagram of the HeBCD H II regions with  $[\text{O III}] \lambda 5007/[\text{O I}] \lambda 6300 > 300$  (Fig. 6d) is  $\sim 20\%$  lower than that for the total HeBCD sample (Fig. 6a), confirming the finding by Ballantyne et al. (2000). However, for the SDSS sample which is larger and hence has better statistics, we do not find that the scatter decreases with increasing value of the cutoff. This suggests that the scatter of points of  $\sim 3\% - 4\%$  around the regression line in Fig. 6 is due mainly to observational statistical uncertainties, and not so much to variations of the  $ICF$ . By contrast with Ballantyne et al. (2000), we find only small changes in  $Y_p$ , by  $\lesssim 0.5\%$ , when the cutoff is increased. These very small  $Y_p$  changes can be due in part to the progressively smaller size of the H II region sample with increasing cutoff, and hence to larger uncertainties in the regression. The nearly constant value of  $Y_p$  implies that  $ICF(\text{He}^+ + \text{He}^{2+})$  is close to the adopted value of unity for our H II regions, regardless of the value of the  $[\text{O III}] \lambda 5007/[\text{O I}] \lambda 6300$  ratio which varies in the range  $\sim 30 - 700$ .

To derive  $ICF(\text{He}^+ + \text{He}^{2+})$ , we use the photoionized H II region models by Stasińska & Izotov (2003), but with an input radiation field computed with Starburst 99 (Leitherer et al. 1999) using the stellar model atmospheres described in Smith et al. (2002). In Fig. 7, we show  $ICF(\text{He}^+ + \text{He}^{2+})$  as a function of the  $\text{O}^{2+}/(\text{O}^+ + \text{O}^{2+})$  abundance ratio, the latter being a measure of the H II region excitation. Filled circles represent low-metallicity H II regions with  $12 + \log \text{O}/\text{H} = 7.2$ , open circles intermediate-metallicity H II regions with  $12 + \log \text{O}/\text{H} = 7.6$  and stars high-metallicity H II regions with  $12 + \log \text{O}/\text{H} = 8.3$ . It is seen from Fig. 7 that the  $ICF$  in low-excitation H II regions, those with low  $\text{O}^{2+}/(\text{O}^+ + \text{O}^{2+})$  abundance ratio, can significantly deviate from unity. However, our sample consists only of high-excitation H II regions with  $\text{O}^{2+}/(\text{O}^+ + \text{O}^{2+}) > 0.5$  and for these objects,  $ICF$  deviates from unity by not more than 1%. In our calculations, we use the  $ICF$ s derived by interpolating or extrapolating in metallicity the values given by the three curves in Fig. 7, for a given  $x(\text{O}^{2+}) = N(\text{O}^{2+})/N(\text{O}^+ + \text{O}^{2+})$ . We find that the effect of ionization structure on the derived  $Y_p$  is small. Neglecting the correction for ionization, i.e. adopting  $ICF(\text{He}^+ + \text{He}^{2+}) = 1$ , we obtain a  $Y_p$  which is only  $\lesssim 0.5\%$  larger than the value derived when the correction for ionization is taken into account (compare Fig. 3l and 3a).

#### 4.7. Deviations from case B recombination

All previous work on the primordial He abundance determination has assumed that case B recombination holds in H II regions. Case B assumes that there exists a balance between the absorption and emission of photons in the resonant Lyman series transitions of hydrogen and helium and that there are no other processes. However in real H II regions, processes

do exist that may disrupt this balance. The first of these processes is the leakage of Lyman line photons from the H II region because of a finite optical depth. The second process is the absorption of UV photons by dust inside the H II region. The third process is line pumping of stellar photons.

Thanks to our large data base, we are able to estimate the effect of the deviations from case B for He I emission lines. This is because some singlet emission lines, such as the He I  $\lambda 5015$  and  $\lambda 7281$  lines, are sensitive to this effect, while other singlet lines, such as the He I  $\lambda 4922$  and  $\lambda 6678$  lines, are much less sensitive (Aller 1984). Therefore, singlet He I emission line flux ratios may be good indicators of deviations from case B. The SDSS H II region sample is particularly important in this regard, because the relatively high spectral resolution of the SDSS spectra allows to separate the He I  $\lambda 5015$  emission line from the strong [O III]  $\lambda 5007$  emission line.

In Fig. 8, we show the dependence of the He I  $\lambda 5015/\lambda 6678$ ,  $\lambda 7281/\lambda 6678$  and  $\lambda 4922/\lambda 6678$  singlet flux ratios on oxygen abundance  $12 + \log O/H$  for the SDSS H II regions. We divide the SDSS objects into two groups: the filled circles represent H II regions with  $EW(H\beta) \geq 100\text{\AA}$  and the open circles those with  $EW(H\beta) < 100\text{\AA}$ . This division allows us to check whether or not deviations of the He I flux ratios from case B are affected by underlying stellar absorption. This effect is expected to be higher in H II regions with low  $EW(H\beta)$ . If it plays a role, then a systematic shift between H II regions with high and low  $EW(H\beta)$  should be present in Fig. 8. The solid and dashed lines in Fig. 8 show respectively the theoretical ratios for cases B and A, in the case of two electron temperatures,  $T_e = 10000$  K and  $T_e = 20000$  K. In panels a) and c), the two lines for case A are nearly indistinguishable. The emission line which is most sensitive to deviations from case B is He I  $\lambda 5015$ . It is seen from Fig. 8a that the He I  $\lambda 5015/\lambda 6678$  flux ratio is systematically lower than the theoretical value for case B. The same is true, but to a lesser extent, for the He I  $\lambda 7281/\lambda 6678$  flux ratio. It is also seen that there is no systematic offset between H II regions with high and low  $EW(H\beta)$ . The situation is different for the He I  $\lambda 4922/\lambda 6678$  flux ratio. There is no statistically significant deviation for H II regions with high  $EW(H\beta)$ , but the ratios for H II regions with low  $EW(H\beta)$  are systematically below the case B theoretical value (Fig. 8c). Thus, underlying absorption does play a role, and its effect is most important for the He I  $\lambda 4922$  emission line. This conclusion is supported by the synthetic spectra of González Delgado et al. (1999) who predict rather high ( $0.3 - 0.8 \text{\AA}$ ) equivalent widths for the He I  $\lambda 4922$  absorption line.

Thus, the He I  $\lambda 5015/\lambda 6678$  and  $\lambda 7281/\lambda 6678$  emission line flux ratios clearly show deviations from case B. It is reasonable to suppose that deviations from case B are also present for hydrogen. However, the overall effect of these H deviations on the derived element

abundances is likely to be small. Cota & Ferland (1988) have considered the effect of case B deviations on hydrogen line emissivities caused by a finite optical depth of the Lyman series lines, the presence of velocity gradients and dust. Applying their results to the low-metallicity H II regions in our sample, we find that effect to be small. This, because of several reasons. First, the Ly $\alpha$  optical depth in our H II regions is likely to be very large, more than  $\sim 10^5$ , as evidenced by the very high H I column densities  $\gtrsim 10^{21}$  cm $^{-2}$  measured in some of our objects (Thuan & Izotov 1997; Kunth et al. 1998). Second, the ratio of the number of dust particles to the number of hydrogen atoms in our objects is more than one order of magnitude lower than the ratio in the interstellar medium of the Galaxy, as shown by Izotov et al. (2006) in their study of SDSS extragalactic H II regions. For low-metallicity H II regions with these characteristics, we find from Figs. 3 and 4 of Cota & Ferland (1988) that the recombination rate for hydrogen is smaller than the rate for case B by not more than 1%. Similar conclusions can be reached for helium.

As for case C which occurs when absorption of stellar photons at the wavelengths of Lyman lines is important (Ferland 1999), our Cloudy (version C06.02) calculations show that this situation does not happen in any significant degree in H II regions such as the ones in our sample.

For the objects considered here, the effects of deviations from case B work in the same direction for both hydrogen and helium. Since the determination of the He abundance involves the ratio of  $N(\text{He})$  to  $N(\text{H})$ , these effects partially compensate each other. In the present paper, we have chosen not to take into account the deviations from case B in the calculation of He abundances. Accounting for them accurately would require a precise photoionization modeling for each individual object which is not feasible, given the large size of our sample. However, it would be interesting to attempt this modeling for a few cases in the future, for checking purposes.

#### 4.8. Effect of different samples

In our previous papers (Izotov, Thuan & Lipovetsky 1994, 1997; Izotov & Thuan 1998b, 2004), we have only considered H II regions from the HeBCD sample, data which we acquired and reduced ourselves. In this section, we consider the effect on the  $Y_p$  value when the H II regions from the SDSS sample, observed and reduced independently by the SDSS team, are added. In Fig. 3j, we show the linear regression  $Y - \text{O}/\text{H}$  obtained with the basic parameter set for the combined HeBCD + SDSS sample. It is seen that SDSS data (open circles) have a larger scatter as compared to the HeBCD data (filled circles) which is expected because of the lower signal-to-noise ratio of the SDSS spectra. However, there is no visible offset



between the two data sets. The derived  $Y_p$  value for the combined sample is close to the one obtained for the basic case (compare Fig. 3a and 3j). The difference in  $Y_p$  is  $\sim 0.5\%$ .

We have also derived the regression line for the SDSS subsample only with the basic parameter set. We obtain  $Y = (0.2459 \pm 0.0021) + (90.60 \pm 13.5) \text{ O/H}$ , as compared to  $Y = (0.2509 \pm 0.0012) + (52.48 \pm 9.0) \text{ O/H}$  for the HeBCD subsample only, with the same parameters (see Fig. 3a). The  $Y_p$ s for the two subsamples are consistent with each other at the  $2\sigma$  level. The SDSS subsample was not designed specifically for the  $Y_p$  problem. The derived lower  $Y_p$  and the steeper slope are due to both the lack of very low-metallicity H II regions and the lower quality spectra in the SDSS sample.

#### 4.9. Budget of systematic errors

Table 5 gives a summary budget of the various systematic errors discussed above. After the important effect of collisional enhancement of the He I lines (not listed in Table 5) which can be, depending on the particular line, larger than 10%, the second most important systematic effect is that of underlying He I stellar absorption, as already emphasized by Izotov & Thuan (1998a). Its effect is  $\lesssim 3\%$ . The remaining systematic effects – temperature fluctuations, collisional excitation of H lines and ionization correction factors – are all  $\lesssim 1\%$ , some increasing  $Y_p$ , and some decreasing it. If we adopt the Benjamin et al. (2002) emissivities as in our previous work, then all systematic effects listed in Table 5 add up to a net increase of  $\lesssim 2\%$ . Thus, the value  $Y_p = 0.243$  obtained by Izotov & Thuan (2004) for the HeBCD sample without considering the systematic effects listed in Table 5 should be increased to  $\sim 0.248$ . This is indeed the case. Examination of the maximum likelihood linear regressions in Table 6 for the entries with Benjamin et al. (2002) emissivities and  $N = 93$  show that  $Y_p = 0.247 \pm 0.001$ , whether O/H is calculated with  $T_e(\text{O III})$  or  $T_e(\text{He}^+)$ . Using the Porter et al. (2005) emissivities increases  $Y_p$  by  $\lesssim 1.7\%$ , so that  $Y_p$  becomes equal to  $\sim 0.251$ .

### 5. The primordial He mass fraction $Y_p$ and the slope $dY/dZ$

To account for the various systematic errors, including those caused by collisional and fluorescent enhancements of He I lines and those summarized in Table 5, we have used a Monte Carlo method as described in §3.3 and applied by Izotov & Thuan (2004) to a selected sample of 7 H II regions. We need to fix some parameters and vary others within “reasonable” ranges. We discuss our choices below.

One of the most important sources of uncertainty concerns the He I emissivities. Changing from the Benjamin et al. (1999) and Benjamin et al. (2002) emissivities to those of Porter et al. (2005) changes  $Y_p$  by  $\sim 1.7\%$ . Because the Porter et al. (2005) emissivities have been calculated with updated atomic data, we will adopt them. But to compare with our previous work, and to assess the change in  $Y_p$  caused by the change in emissivities, we have also derived  $Y_p$  with Benjamin et al. (2002) emissivities. As for the equivalent widths of He I stellar absorption lines, we adopt the basic ones (§3.4). This set of equivalent widths appears to be the most reasonable for the reasons discussed in §4.4 and also because it gives the lowest  $\chi^2_{min}$  for the derived  $Y$ s in individual H II regions. For  $T_e(\text{He}^+)$ , variations in the range  $(0.95 - 1.0) \times T_e(\text{O III})$  appear to be reasonable and are consistent with the measurements of Guseva et al. (2006, 2007). We vary  $N_e(\text{He}^+)$  and  $\tau(\lambda 3889)$  in the ranges  $10 - 450 \text{ cm}^{-3}$  and  $0 - 5$ . The ionization correction factor  $ICF(\text{He}^+ + \text{He}^{2+})$  is interpolated or extrapolated from the curves in Fig. 7.

In Table 3 (available only in electronic form), we show for the whole HeBCD+SDSS sample oxygen abundances O/H and nitrogen abundances N/H calculated for two different cases, one where the electron temperature  $T_e$  is set to  $T_e(\text{O III})$  and one where it is set to  $T_e(\text{He}^+)$ , and He mass fractions  $Y$ . Table 4 (also in electronic form only) shows the values of the parameters with which the abundances in Table 3 are calculated.

Linear regressions  $Y - \text{O/H}$  and  $Y - \text{N/H}$  for the HeBCD sample calculated with the Benjamin et al. (2002) He I emissivities are shown in Fig. 9, in the cases where  $\text{O/H} = \text{O/H}[T_e(\text{O III})]$  (Fig. 9a,b) and  $\text{O/H} = \text{O/H}[T_e(\text{He}^+)]$  (Fig. 9c,d). The corresponding regression lines calculated with the Porter et al. (2005) He I emissivities are shown in Fig. 10. Comparison of Figs. 9 and 10 shows that  $Y_p$  does not depend sensitively on whether O/H is computed with an electron temperature equal to  $T_e(\text{O III})$  or  $T_e(\text{He}^+)$ , while the slope  $dY/d(\text{O/H})$  is quite sensitive to the adopted  $T_e$ . This is because  $Y_p$  is determined mainly by low-metallicity H II regions for which changes in O/H caused by different  $T_e$  are small compared to the whole O/H range for the sample. On the other hand,  $dY/d(\text{O/H})$  is mainly determined by high-metallicity H II for which changes in O/H caused by different temperatures are comparable to the whole O/H range. The same is true for the  $Y - \text{N/H}$  linear regressions.

From the  $Y - \text{O/H}$  regressions for the HeBCD sample with the Benjamin et al. (2002) and Porter et al. (2005) He I emissivities and  $\text{O/H} = \text{O/H}[T_e(\text{He}^+)]$ , we obtain respectively  $Y_p = 0.2472 \pm 0.0012$  and  $0.2516 \pm 0.0011$  (Fig. 9c, 10c). The parameters of the regression lines are also given in Table 6. The values of  $Y_p$  obtained from the  $Y - \text{N/H}$  linear regressions (Fig. 9d, 10d, Table 6) are higher, being respectively  $Y_p = 0.2489 \pm 0.0009$  and  $Y_p = 0.2532 \pm 0.0009$  for the Benjamin et al. (2002) and Porter et al. (2005) He I emissivities.

As noted before (e.g. Izotov & Thuan 2004, and references therein), the systematically higher  $Y_p$  from the  $Y - N/H$  regression is due to the nonlinear dependence of the nitrogen abundance on oxygen abundance. This makes the  $Y - N/H$  linear regression less reliable for the determination of  $Y_p$ .

For comparison, the linear regressions for the total HeBCD + SDSS sample with the Benjamin et al. (2002) and Porter et al. (2005) He I emissivities are shown respectively in Figs. 11 and 12. The HeBCD H II regions are represented by filled circles and the SDSS H II regions by open circles. Using the  $Y - O/H$  linear regressions, we obtain  $Y_p = 0.2457 \pm 0.0010$  (Fig. 11c) when Benjamin et al. (2002) emissivities are used and  $Y_p = 0.2505 \pm 0.0010$  (Fig. 12c) when Porter et al. (2005) emissivities are used. The  $Y_p$ s derived for the HeBCD+SDSS sample are consistent within the errors with the ones derived from the HeBCD sample alone (compare the regression parameters in Table 6, where the total sample is characterized by  $N = 364$  H II regions, and the HeBCD sample by  $N = 93$  H II regions). As can be seen from Figures 11 and 12, the scatter about the regression lines is considerably larger for the SDSS sample than for the HeBCD sample. Thus since the data points entering in the determination of the regression lines are weighted by their errors, most of the weight in the  $Y_p$  determination still comes from the HeBCD sample, even in the total HeBCD+SDSS sample. Going from 93 to 364 H II regions does not change appreciably the  $1\sigma$  error in the determination of  $Y_p$ : it decreases only by 0.0001. Thus, while we show the results for the total sample for comparison, we consider the  $Y_p$  determined from the HeBCD sample, for which we understand well the selection effects, as being the best value.

Using Eq. 4, we derive from the  $Y - O/H$  linear regressions (Table 6) the slopes  $dY/dZ = 2.38 \pm 0.45$  and  $2.19 \pm 0.39$  for the HeBCD sample, in the case where  $O/H$  is calculated with  $T_e(\text{He}^+)$ , and for the Benjamin et al. (2002) and Porter et al. (2005) He I emissivities respectively (Fig. 11c, 12c). These slopes are steeper than the ones predicted by closed-box chemical evolution models of dwarf galaxies ( $\sim 1$ , Larsen et al. 2001). It is reasonable to expect that some fraction of chemical elements, especially oxygen, escapes the galaxy due to e.g. supernova explosions. The slopes  $dY/dZ$  derived from the  $Y - N/H$  linear regressions (Fig. 11d, 12d) are not as steep:  $dY/dZ = 1.46 \pm 0.25$  and  $1.34 \pm 0.24$  respectively for the Benjamin et al. (2002) and Porter et al. (2005) He I emissivities, and for the case where  $O/H$  is calculated with  $T_e(\text{He}^+)$ . Again, the difference is due to the nonlinear dependence of the N abundance on O abundance, as discussed above. As for  $Y_p$ , this makes the determination of  $dY/dZ$  from the  $Y - N/H$  regression not as reliable as the one from the  $Y - O/H$  regression. The  $dY/dZ$  slopes are steeper when  $T_e(\text{O III})$  is used for the  $O/H$  determination. In the latter case, we obtain for the HeBCD sample, from the  $Y - O/H$  regressions,  $dY/dZ = 2.94 \pm 0.51$  and  $2.88 \pm 0.50$  respectively for the two sets of emissivities (Fig. 11a and 12a). The true electron temperature is probably somewhere between  $T_e(\text{He}^+)$  and  $T_e(\text{O III})$ , so

we expect the true slopes to be in the range 2.2 – 2.9 for both Benjamin et al. (2002) and Porter et al. (2005) emissivities.

Our  $Y_p$  range of  $\sim 0.001$  is much smaller than the one of  $\sim 0.009$  claimed by Olive & Skillman (2004). This difference is due to 1) different methods used in this paper and in Olive & Skillman (2004) and 2) much larger samples used in this paper (93 observations in the HeBCD sample and 364 observations in the total sample as compared to 7 objects in the Olive & Skillman (2004) sample). We emphasize that the use of large sample significantly reduces the uncertainties in  $Y_p$  to the level that is acceptable for cosmological implications.

## 6. COSMOLOGICAL IMPLICATIONS

### 6.1. The baryonic mass density

We now investigate whether our derived values of  $Y_p$  are consistent with the predictions of SBBN and whether the baryonic mass density corresponding to  $Y_p$  agrees with the one derived from measurements of the CMB. In Fig. 13, we show by solid curves the dependence of the abundances of the three light elements He, D and  $^7\text{Li}$  on the baryon-to-photon number ratio  $\eta$  as predicted by SBBN (e.g. Steigman 2006). We do not discuss  $^3\text{He}$  because the derivation of its primordial value from its presently observed value in the Galaxy is complicated by uncertain effects of chemical evolution. The solid and dashed vertical lines show the value of  $\eta$  and its  $1\sigma$  deviations as obtained by WMAP (Spergel et al. 2006). The presently best observational abundances of the three light elements with their  $1\sigma$  deviations are shown by boxes. Concerning He, we show in the left and right panels the  $Y_p$  derived from regression fitting of the HeBCD sample and with O/H obtained respectively with the electron temperature set equal to  $T_e(\text{O III})$  and  $T_e(\text{He}^+)$ . We shall discuss the results concerning our preferred values of  $Y_p$ , the ones corresponding to  $T_e = T_e(\text{He}^+)$ . With  $Y_p = 0.2472 \pm 0.0012$  and  $0.2516 \pm 0.0011$  (solid boxes in Fig. 13d) for the two different sets of He I emissivities, and with an equivalent number of light neutrino species equal to 3, the SBBN model gives  $\eta_{10} = 10^{10}\eta = 5.5^{+0.7}_{-0.6}$  and  $8.7^{+1.1}_{-1.0}$ , respectively, where the error bars denote  $1\sigma$  errors. These values correspond to a baryonic mass fractions  $\Omega_b h^2 = 0.020^{+0.003}_{-0.002}$  and  $0.032^{+0.004}_{-0.004}$  respectively for Benjamin et al. (2002) and Porter et al. (2005) He I emissivities. The value derived with the old Benjamin et al. (2002) He I emissivities is much higher than  $\Omega_b h^2$  derived from the primordial  $^7\text{Li}$  abundance (Bonifacio & Molaro 1997; Asplund et al. 2006; Bonifacio et al. 2007) but is in excellent agreement with  $\Omega_b h^2 = 0.021 \pm 0.002$  derived from recent measurements of the deuterium abundance in damped Ly $\alpha$  systems (Kirkman et al. 2003; O’Meara et al. 2006) and  $\Omega_b h^2 = 0.0223 \pm 0.0008$  derived from measurements of the fluctuations of the microwave background radiation by WMAP (Spergel et al. 2006). An-

other way of saying the same thing is that the observational value of  $Y_p$  derived with the Benjamin et al. (2002) He I emissivities is in excellent agreement with the theoretical SBBN value of 0.248.

On the other hand, the  $Y_p$  derived with the new Porter et al. (2005) He I emissivities is larger than the predicted SBBN value and is only consistent with it at the  $2\sigma$  level. Consequently, the corresponding  $\Omega_b h^2 = 0.032^{+0.004}_{-0.004}$  is also consistent only at the  $2\sigma$  level with the value inferred from the D abundance measurements and the WMAP data. In principle, the Porter et al. (2005) He I emissivities should be more reliable than those from Benjamin et al. (2002), since they are based on new updated atomic data for He.

Steigman (2006) has shown that, while He may not be as sensitive a baryometer as D, it is an excellent chronometer (in the sense that it is sensitive to small deviations from the standard Hubble expansion rate) and/or leptometer (in the sense that it is sensitive to any asymmetry between the numbers of neutrinos and antineutrinos). We investigate next possible small deviations from SBBN if we take at face value the relatively high value of  $Y_p$  obtained with the Porter et al. (2005) He I emissivities.

## 6.2. Deviations from SBBN

Deviations from the standard rate of Hubble expansion in the early Universe can be caused by an extra contribution to the total energy density (for example by additional flavors of active or sterile neutrinos) which can conveniently be parameterized by an equivalent number of neutrino flavors  $N_\nu$ . Combining  $\Omega_b h^2 = 0.00223 \pm 0.0008$  obtained by WMAP (Spergel et al. 2003) with  $Y_p = 0.2516 \pm 0.0011$ , we obtain  $N_\nu \sim 3.2$  (Walker et al. 1991).

We use the statistical  $\chi^2$  technique with the code described by Fiorentini et al. (1998) and Lisi et al. (1999) to analyze the constraints that the measured He, D and  $^7\text{Li}$  abundances put on  $\eta$  and  $N_\nu$ . For the primordial D and  $^7\text{Li}$  abundances, we use respectively the values obtained by O’Meara et al. (2006) and Asplund et al. (2006). With  $Y_p = 0.2472 \pm 0.0012$  (emissivities by Benjamin et al. 2002), the minimum  $\chi^2_{min} = 9.036$  is obtained when  $\eta_{10} = 5.79$  and  $N_\nu = 2.972$ . With  $Y_p = 0.2516 \pm 0.0011$  (emissivities by Porter et al. 2005), the minimum  $\chi^2_{min} = 9.334$  is obtained when  $\eta_{10} = 5.97$  and  $N_\nu = 3.280$ .

The joint fits of  $\eta$  and  $N_\nu$  with the  $Y_p$ s derived with the two sets of emissivities are shown respectively in Figure 14a and 14b. The  $1\sigma$  ( $\chi^2 - \chi^2_{min} = 1.0$ ) and  $2\sigma$  ( $\chi^2 - \chi^2_{min} = 2.71$ ) deviations are shown respectively by the thin and thick solid lines. We find the equivalent number of light neutrino species to be respectively in the range  $N_\nu = 2.97 \pm 0.16$  ( $2\sigma$ ) (Fig. 14a), and  $N_\nu = 3.28 \pm 0.16$  ( $2\sigma$ ) (Fig. 14b). The first value of  $N_\nu$  obtained with

$Y_p$  derived with the old set of He I emissivities is entirely consistent with the experimental value of  $2.993 \pm 0.011$  (Caso et al. 1998) shown by the dashed line. On the other hand, the second value of  $N_\nu$  obtained with  $Y_p$  derived with the new set of He I emissivities is significantly higher than the experimental value, suggesting a slight deviation from SBBN. We note that the primordial helium abundance sets very tight constraints on the effective number of neutrino species. These constraints are much tighter than those derived using the CMB and galaxy clustering power spectra. For example, using these two sets of data, Ichikawa et al. (2006) derive  $0.8 < N_\nu < 7.6$  at the 95% confidence level.

Alternatively, deviations from the SBBN model can be checked by introducing two parameters, the expansion rate parameter  $S$ , and the electron neutrino asymmetry parameter  $\xi_e$ , as suggested by Steigman (2005). If deviations from the standard expansion are caused by an extra non-standard energy density component, then it is convenient to express that extra energy component in terms of an extra effective number of neutrino species  $\Delta N_\nu$  defined as:  $N_\nu = 3 + \Delta N_\nu$ . Then  $S$  is related to  $\Delta N_\nu$  by:

$$S = \left(1 + \frac{7}{43} \Delta N_\nu\right)^{1/2}. \quad (13)$$

For the SBBN model,  $\Delta N_\nu = 0$ ,  $N_\nu = 3$  and  $S = 1$ .

As for the parameter  $\xi_e$ , it is related to the difference between the number of electron neutrino species  $n_{\nu_e}$  and the number of electron antineutrino species  $n_{\bar{\nu}_e}$  by :

$$\xi_e \approx 1.33 \left( \frac{n_{\nu_e} - n_{\bar{\nu}_e}}{n_\gamma} \right), \quad (14)$$

where  $n_\gamma$  is the number of photons. A non-zero  $\xi_e$  would result in a different n/p ratio during the BBN period, therefore changing the light element abundances. In particular, if  $\xi_e > 0$ , there are more neutrinos than antineutrinos, and reactions such as  $n + \nu_e \rightarrow p + e^-$  drive down the n/p ratio (Steigman 2005).

Following Steigman (2005), we show in Fig. 15a the  $S - \eta$  diagram with the nearly orthogonal isoabundance curves of D (dashed lines) and He (solid lines), in the case where  $\xi_e = 0$ . The open circle corresponds to the value of the primordial D/H abundance ratio derived by O’Meara et al. (2006) and that of the primordial He mass fraction derived in this paper, using the Benjamin et al. (1999) He I emissivities. The filled circle corresponds to the same D/H abundance ratio, but to  $Y_p$  derived with the Porter et al. (2005) He I emissivities. From Fig. 15a, we obtain  $S = 0.996 \pm 0.007$  ( $1\sigma$ ) and  $1.020 \pm 0.006$  ( $1\sigma$ ) for  $Y_p$  obtained respectively with the old and new He I emissivities. As before, we find that the first value is consistent within the errors with the SBBN value,  $S = 1$ . On the other hand, the second value indicates a slight deviation from the SBBN and implies the presence

of additional neutrino species. The same conclusion can be reached with Fig. 15b. It shows the  $\xi_e - \eta$  diagram with the isoabundances curves of D (dashed lines) and He (solid lines), in the case where  $S = 1$ . Again, it can be seen that the  $Y_p$  derived with the Benjamin et al. (1999) He I emissivities is consistent with SBBN ( $\xi_e = 0$ ), while the  $Y_p$  derived with the Porter et al. (2005) He I emissivities gives a negative value of  $\xi_e$ , indicating deviation from SBBN.

## 7. SUMMARY AND CONCLUSIONS

We present in this paper the determination of the primordial helium mass fraction  $Y_p$  by linear regressions of a sample of 93 spectra of 86 H II low-metallicity extragalactic regions (the HeBCD sample). This sample is one of the largest and most homogeneous data sets in existence for the determination of  $Y_p$ . For comparison and to improve the statistics for investigating systematic effects in the determination of  $Y_p$ , we have also considered a sample of 271 low-metallicity H II regions selected from the Data Release 5 of the Sloan Digital Sky Survey (the SDSS sample).

In the determination of  $Y_p$ , we have considered several known systematic effects. We have used Monte Carlo methods to take into account the effects of collisional and fluorescent enhancements of He I recombination lines, of collisional excitation of hydrogen emission lines, of underlying stellar He I absorption, of the difference between the temperature  $T_e(\text{He}^+)$  in the  $\text{He}^+$  zone and the temperature  $T_e(\text{O III})$  derived from the  $[\text{O III}]\lambda 4363/(\lambda 4959 + \lambda 5007)$  flux ratio, and of the ionization correction factor  $ICF(\text{He}^+ + \text{He}^{2+})$ . We have also considered the effects of different sets of He I line emissivities and of different reddening laws. We discuss the effect of possible deviations of He I and H emission line intensities from case B.

We have obtained the following results:

1. After the effect of collisional enhancement of the He I lines, the second most important systematic effect comes from underlying He I stellar absorption ( $\sim 3\%$ ). Other effects such as variations in temperature, collisional excitation of hydrogen emission lines or ionization corrections are smaller ( $\sim 1\%$ ). Because those systematic effects can work in either direction, either increasing or decreasing  $Y_p$ , they tend to cancel each other, so that the net effect of all the considered systematic effects is an increase of  $Y_p$  of  $\sim 2\%$  as compared to the value derived by Izotov & Thuan (2004). With the old set of He I emissivities by Benjamin et al. (2002) used by Izotov & Thuan (2004), and with the electron temperature set, not to  $T_e(\text{O III})$ , but to  $T_e(\text{He}^+)$ , we derive  $Y_p = 0.2472 \pm 0.0012$  which, according to SBBN, corresponds to a baryonic mass fraction  $\Omega_b h^2 = 0.020^{+0.003}_{-0.002}$ . This value of  $\Omega_b h^2$  is consistent with the ones

derived from deuterium abundance observations and WMAP microwave background radiation fluctuation measurements, and all three measurements concur to support the validity of the SBBN model (SBBN predicts  $Y_p = 0.248$  when  $\Omega_b h^2$  is set to the value derived by WMAP, Spergel et al. 2006). We have checked that the derived  $Y_p$  does not depend on the particular sample of H II regions used. We have also performed regression fits for the SDSS sample observed and reduced by the Sloan team, and found that the derived  $Y_p$  is consistent at the  $2\sigma$  level with the value obtained from the HeBCD sample.

2. On the other hand, if the new set of emissivities, based on updated He I atomic data, by Porter et al. (2005) is used, then we obtain  $Y_p = 0.2516 \pm 0.0011$ , corresponding to  $\Omega_b h^2 = 0.032^{+0.004}_{-0.004}$ , significantly larger (at the  $2\sigma$  level) than the  $\Omega_b h^2$  values derived from the deuterium abundance and microwave background radiation fluctuation measurements. If we take the higher value of  $Y_p$  at its face value, then this would imply the existence of small deviations from SBBN. In order to bring the high value of  $Y_p$  into agreement with the deuterium and WMAP measurements, we would need an equivalent number of neutrino flavors equal to 3.303 instead of the canonical 3.

3. The  $dY/dZ$  slopes derived from the  $Y - O/H$  linear regressions for the HeBCD sample, using He I emissivities by Benjamin et al. (2002) and Porter et al. (2005), are respectively equal to  $2.38 \pm 0.45$  and  $2.19 \pm 0.39$ , consistent with previous determinations by Izotov, Thuan & Lipovetsky (1997), Izotov & Thuan (1998b, 2004) using BCDs, and by Jimenez et al. (2003) from nearby K dwarf stars.

We have considered here, as best as we can, all known systematic uncertainties that may affect the determination of the primordial He abundance. However, the real situation may be more complicated. The most important issue that we do not yet fully understand appears to be the temperature structure of H II regions. For example, detailed photoionization models of H II regions often underpredict the electron temperature that is measured from the  $[O III] \lambda 4363 / (\lambda 4959 + \lambda 5007)$  line ratio (see e.g. references in Luridiana et al. 2003). Also, there are indications that the matter inside H II regions is not chemically homogeneous (Tsamis & Péquignot 2005, Stasińska et al, in preparation), so that the oxygen abundance obtained by traditional H II region abundance analysis may be biased. How much this affects the He/H abundance ratio, as well as the slope in the  $Y$  vs  $O/H$  relation is not known yet. Finally, as suggested long ago by Bond et al. (1983), very massive primordial stars may produce a significant amount of helium without overproducing metals, in which case the primordial helium abundance could be smaller than obtained from a linear extrapolation of the  $Y - O/H$  relation. Recent computations of Population III star yields (Marigo et al. 2003) associated with measurements of the near-infrared background suggest that this may be the case (Salvaterra & Ferrara 2003).



Y.I.I. is grateful to the staff of the Astronomy Department at the University of Virginia for warm hospitality. He thanks the support of the Deutsche Forschung Gesellschaft (DFG) grant No. 436 UKR 17/25/05. Y.I.I. and T.X.T. thank the support of National Science Foundation grant AST 02-05785. The research described in this publication was made possible in part by Award No. UP1-2551-KV-03 of the US Civilian Research & Development Foundation for the Independent States of the Former Soviet Union (CRDF). All the authors acknowledge the work of the Sloan Digital Sky Survey (SDSS) team. Funding for the SDSS has been provided by the Alfred P. Sloan Foundation, the Participating Institutions, the National Aeronautics and Space Administration, the National Science Foundation, the U.S. Department of Energy, the Japanese Monbukagakusho, and the Max Planck Society. The SDSS Web site is <http://www.sdss.org/>. The SDSS is managed by the Astrophysical Research Consortium (ARC) for the Participating Institutions. The Participating Institutions are The University of Chicago, Fermilab, the Institute for Advanced Study, the Japan Participation Group, The Johns Hopkins University, the Korean Scientist Group, Los Alamos National Laboratory, the Max-Planck-Institute for Astronomy (MPIA), the Max-Planck-Institute for Astrophysics (MPA), New Mexico State University, University of Pittsburgh, University of Portsmouth, Princeton University, the United States Naval Observatory, and the University of Washington.

## REFERENCES

- Adelman-McCarthy, J. K., Agüeros, M. A., Allam, S. S., et al. 2006, *ApJS*, 162, 38
- Aller, L. H. 1984, *Physics of Thermal Gaseous Nebulae* (Dordrecht: Reidel)
- Anderson, H., Ballance, C. P., Badnell, N. R., & Summers, H. P. 2002, *J. Phys. B: At. Mol. Opt. Phys*, 35, 1613
- Asplund, M., Lambert, D. L., Nissen, P. E., Primas, F., & Smith, V. V. 2006, *ApJ*, 644, 229
- Ballantyne, D. R., Ferland, G. J., & Martin, P. G. 2000, *ApJ*, 536, 773
- Bania, T. M., Rood, R. T., & Balser, D. S. 2002, *Nature*, 415, 54
- Barger, V., Kneller, J. P., Lee, H.-S., Marfatia, D., & Steigman, G. 2003a, *Physics Letters B*, 566, 8
- Barger, V., Kneller, J. P., Langacker, P., Marfatia, D., & Steigman, G. 2003b, *Physics Letters B*, 569, 123
- Bauman, R. P., Porter, R. L., Ferland, G. J., & MacAdam, K. B. 2005, *ApJ*, 628, 541

- Benjamin, R. A., Skillman, E. D., & Smits, D. P. 1999, *ApJ*, 514, 307
- . 2002, *ApJ*, 569, 288
- Binette, L., & Luridiana, V. 2000, *Rev. Mexicana Astron. Astrofis.*, 36, 43
- Bond, J. R., Carr, B. J., & Arnett, W. D. 1983, *Nature*, 304, 514
- Bonifacio, P., & Molaro, P. 1997, *MNRAS*, 285, 847
- Bonifacio, P., Molaro, P., Sivarani, T., et al. 2007, *A&A*, 462, 851
- Burles, S., & Tytler, D. 1998a, *ApJ*, 499, 699
- . 1998b, *ApJ*, 507, 732
- Cardelli, J. A., Clayton, G. C., & Mathis, J. S. 1989, *ApJ*, 345, 245
- Caso, C., et al. (Particle Data Group) 1998, *Eur. J. Phys.*, C3, 1
- Charbonnel, C., & Primas, F. 2005, *A&A*, 442, 961
- Chen, X., Scherrer, R. J., & Steigman, G. 2001, *Phys. Rev. D*, 2001, 6313504
- Cota, S. A., & Ferland, G. J. 1988, *ApJ*, 326, 889
- Crighton, N. H. M., Webb, J. K., Ortiz-Gil, A., & Fernández-Soto, A. 2004, *MNRAS*, 355, 1042
- Cyburt, R. H., Fields, B. D., Olive, K. A., & Skillman, E. D. 2005, *Astroparticle Physics*, 23, 313
- Davidson, K., & Kinman, T. D. 1985, *ApJS*, 58, 321
- Dinerstein, H. L., & Shields, G. A. 1986, *ApJ*, 311, 45
- Esteban, C., Peimbert, M., Torres-Peimbert, S., & Escalante, V. 1998, *MNRAS*, 295, 301
- Ferland, G. J. 1999, *PASP*, 111, 1524
- Fiorentini, G., Lisi, E., Sarkar, S., & Villante, F. L. 1998, *Phys. Rev. D*, 58, 063506
- Fukugita, M., & Kawasaki, M. 2006, *ApJ*, 646, 691
- Garcia-Rojas, J., Esteban, C., Peimbert, A., Peimbert, M., Rodriguez, M., & Ruiz, M. T. 2004, *ApJS*, 2004, 153, 501

- Garcia-Rojas, J., Esteban, C., Peimbert, M., Rodriguez, M., Ruiz, M. T., & Peimbert, A. 2005, *MNRAS*, 362, 301
- Gonzalez-Delgado, R. M., Perez, E., Tenorio-Tagle, G., et al. 1994, *ApJ*, 437, 239
- González Delgado, R. M., Leitherer, C., & Heckman, T. M. 1999, *ApJS*, 125, 489
- Gruenwald, R., Steigman, G., & Viegas, S. M. 2002, *ApJ*, 567, 931
- Guseva, N. G., Izotov, Y. I., & Thuan, T. X. 2006, *ApJ*, 644, 890
- Guseva, N. G., Izotov, Y. I., Papaderos, P., & Fricke, K. J. 2007, *A&A*, in press; preprint astro-ph/0701032
- Hummer, D. G., & Storey, P. J. 1992, *MNRAS*, 254, 277
- Ichikawa, K., Kawasaki, M., & Takahashi, F. 2006, in press; preprint astro-ph/0611784
- Izotov, Y. I., & Thuan, T. X. 1998a, *ApJ*, 497, 227
- . 1998b, *ApJ*, 500, 188 (IT98)
- . 1999, *ApJ*, 511, 639
- . 2004, *ApJ*, 602, 200 (IT04)
- Izotov, Y. I., Thuan, T. X., & Lipovetsky, V. A. 1994, *ApJ*, 435, 647
- . 1997a, *ApJS*, 108, 1
- Izotov, Y. I., Chaffee, F. H., Foltz, C. B., Green, R. F., Guseva, N. G., & Thuan, T. X. 1999, *ApJ*, 527, 757
- Izotov, Y. I., Stasińska, G., Meynet, G., Guseva, N. G., & Thuan, T. X. 2006, *A&A*, 448, 955
- Jimenez, R., Flynn, C., MacDonald, J., & Gibson, B. K. 2003, *Science*, 299, 1552
- Kirkman, D., Tytler, D., Suzuki, N., O’Meara, J. M., & Lubin, D. 2003, *ApJS*, 149, 1
- Kneller, J. P., Scherrer, R. J., Steigman, G., & Walker, T. P. 2001, *Phys. Rev. D*, 6413506
- Kunth, D., & Sargent, W. L. W. 1983, *ApJ*, 273, 81
- Kunth, D., Mas-Hesse, J. M., Terlevich, E., Terlevich, R., Lequeux, J., & Fall, S. M. 1998, *A&A*, 334, 11

- Larsen, T. I., Sommer-Larsen, J., & Pagel, B. E. J. 2001, *MNRAS*, 323, 555
- Leitherer, C., Schaerer, D., Goldader, J. D., Gonzalez Delgado, R. M., Robert, C., Kune D. F., de Mello, D. F., Devost, D., & Heckman, T. M. 1999, *ApJS*, 123, 3
- Lisi, E., Sarkar, S., & Villante, F. L. 1999, *Phys. Rev. D*, 59, 123520
- Luridiana, V., Peimbert, A., Peimbert, M., & Cerviño, M. 2003, *ApJ*, 592, 846
- Maeder, A. 1992, *A&A*, 264, 105
- Marigo, P., Chiosi, C., & Kudritzki, R.-P. 2003, *A&A*, 399, 617
- Mathis, J. S. 1995, *Rev. Mexicana Astron. Astrofis.*, 3, 207
- Netterfield, C. B., Ade, P. A. R., Bock, J. J., et al. 2002, *ApJ*, 571, 604
- Oke, J. B. 1990, *AJ*, 99, 1621
- Olive, K. A., & Skillman, E. D. 2001, *New A*, 6, 119
- . 2004, *ApJ*, 617, 29
- Olive, K. A., & Steigman, G. 1995, *ApJS*, 97, 49
- Olive, K. A., Skillman, D. A., & Steigman, G. 1997, *ApJ*, 483, 788
- Olofsson, K. 1995, *A&AS*, 111, 57
- O’Meara, J. M., Tytler, D., Kirkman, D., Suzuki, N., Prochaska, J. X., Lubin, D., & Wolfe, A. M. 2001, *ApJ*, 552, 718
- O’Meara, J. M., Burles, S., Prochaska, J., Prochter, G. E., Bernstein, R. A., & Burgess, K. M. 2006, *ApJ*, 649, 61
- Pagel, B. E. J., Simonson, E. A., Terlevich, R. J., & Edmunds, M. G. 1992, *MNRAS*, 255, 325
- Peimbert, A. 2003, *ApJ*, 584, 735
- Peimbert, A., Peimbert, M., & Luridiana, V. 2002, *ApJ*, 565, 668
- Peimbert, M. 1967, *ApJ*, 150, 825
- Peimbert, M., & Torres-Peimbert, S. 1974, *ApJ*, 193, 327

- . 1976, *ApJ*, 203, 581
- Peimbert, M., Storey, P.J., & Torres-Peimbert, S. 1993, *ApJ*, 414, 626
- Peimbert, M., Peimbert, A., & Ruiz, M. T. 2000, *ApJ*, 541, 688
- Peña, M. 1986, *PASP*, 98, 1061
- Pettini, M., & Bowen, D. W. 2001, *ApJ*, 560, 41
- Porter, R. L., Bauman, R. P., Ferland, G. J., & MacAdam, K. B. 2005, *ApJ*, 622, L73
- Porter, R. L., Ferland, G. J., & MacAdam, K. B. 2006, *ApJ*, in press; preprint astro-ph/0611579
- Press, W. H., Teukolsky, S. A., Vetterling, W. T., & Flannery, B. P., 1992, *Numerical Recipes in C, The Art of Scientific Computing /Second Edition/*, Cambridge University Press
- Pryke, C., Halverson, N. W., Leitch, E. M., Kovac, J., Carlstrom, J. E., Holzzapfel, W. L., & Dragovan, M. 2002, *ApJ*, 568, 46
- Rayo, J. F., Peimbert, M., & Torres-Peimbert, S. 1982, *ApJ*, 255, 1
- Salvaterra, R., & Ferrara, A. 2003, *MNRAS*, 340, L17
- Sauer, D., & Jedamzik, K. 2002, *A&A*, 381, 361
- Smith, L. J., Norris, R. P. F., & Crowther, P. A., 2002, *MNRAS*, 337, 1309
- Spergel, D. N., Verde, L., Peiris, H. V., et al. 2003, *ApJS*, 148, 175
- Spergel, D. N., Bean, R., Doré, O., et al. 2006, *ApJ*, in press; preprint astro-ph/0603449
- Stasińska, G. 1980, *A&A*, 84, 320
- Stasińska, G., & Izotov, Y. I. 2001, *A&A*, 378, 817
- . 2003, *A&A*, 397, 71
- Stasińska, G., & Schaerer, D. 1999, *A&A*, 351, 72
- Steigman, G. 2005, *Phys. Scr*, T121, 142
- . 2006, *Int. J. Mod. Phys. E*, 15, 1
- Steigman, G., Viegas, S. M., & Gruenwald, R. 1997, *ApJ*, 490, 187

- Tegmark, M., Blanton, M. R., Strauss, M. A., et al. 2004, *ApJ*, 606, 702
- Thuan, T. X., & Izotov, Y. I. 1997, *ApJ*, 489, 623
- . 2005, *ApJS*, 161, 240
- Thuan, T. X., Izotov, Y. I., & Lipovetsky, V. A. 1995, *ApJ*, 445, 108
- Tsamis, Y. G., & Péquignot, D. 2005, *MNRAS*, 364, 687
- Viegas, S. M., Gruenwald, R., & Steigman, G. 2000, *ApJ*, 531, 813
- Walker, T. P., Steigman, G., Kang, H. S., Schramm, D. M., & Olive, K. A. 1991, *ApJ*, 376, 51
- Whitford, A. E. 1958, *AJ*, 63, 201
- York, D. G., Adelman, J., Anderson, J. E., Jr., et al. 2000, *AJ*, 120, 1579

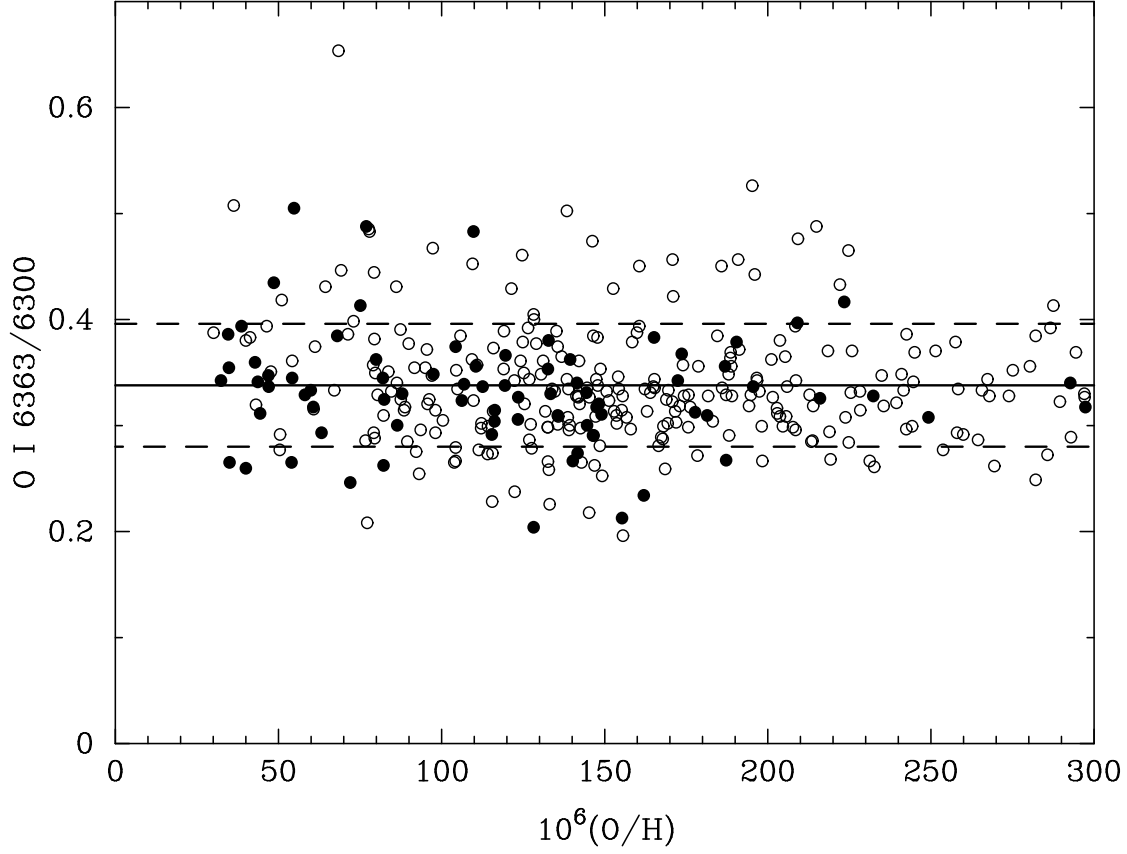


Fig. 1.—  $[\text{O I}] \lambda 6363/\lambda 6300$  emission line flux ratio vs oxygen abundance. The HeBCD and SDSS galaxies are shown respectively by filled and open circles. The solid line shows the mean value of the  $[\text{O I}] \lambda 6363/\lambda 6300$  emission line flux ratio and the dashed lines  $1\sigma$  deviations from the mean.

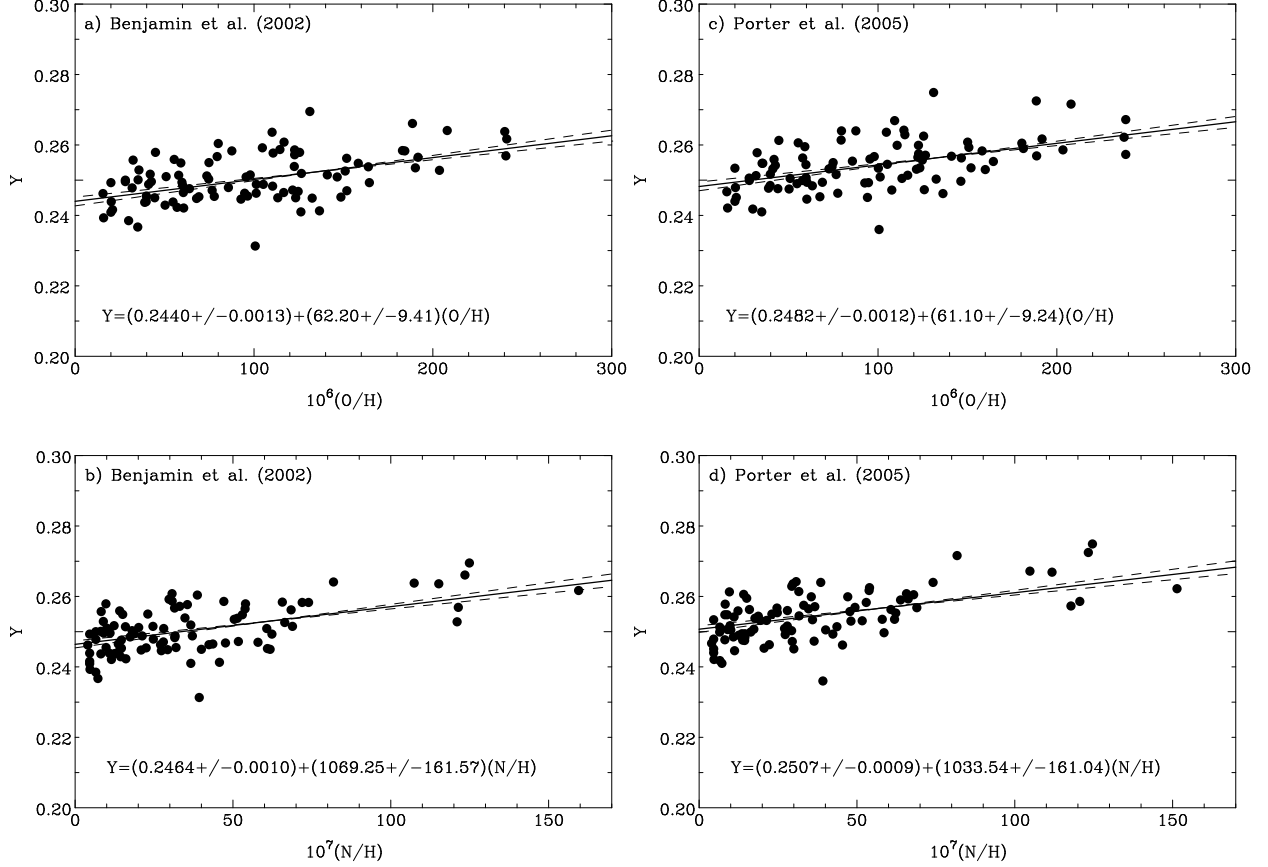


Fig. 2.— Linear regressions of the helium mass fraction  $Y$  vs. oxygen and nitrogen abundances for H II regions in the HeBCD sample. The He I emissivities in (a) and (b) are from Benjamin et al. (1999, 2002) and in (c) and (d) from Porter et al. (2005). In all panels,  $Y$  was derived by minimizing  $\chi^2$  and adopting  $EW_{abs}(\lambda 4471) = 0.4 \text{ \AA}$ ,  $EW_{abs}(\lambda 3889) = EW_{abs}(\lambda 4471)$ ,  $EW_{abs}(\lambda 5876) = 0.3 \times EW_{abs}(\lambda 4471)$ ,  $EW_{abs}(\lambda 6678) = EW_{abs}(\lambda 7065) = 0.1 \times EW_{abs}(\lambda 4471)$ . The electron temperature  $T_e(\text{He}^+)$  is varied in the range  $(0.90 - 1.00) \times T_e(\text{O III})$ . The oxygen and nitrogen abundances are calculated setting the electron temperature equal to  $T_e(\text{O III})$ .



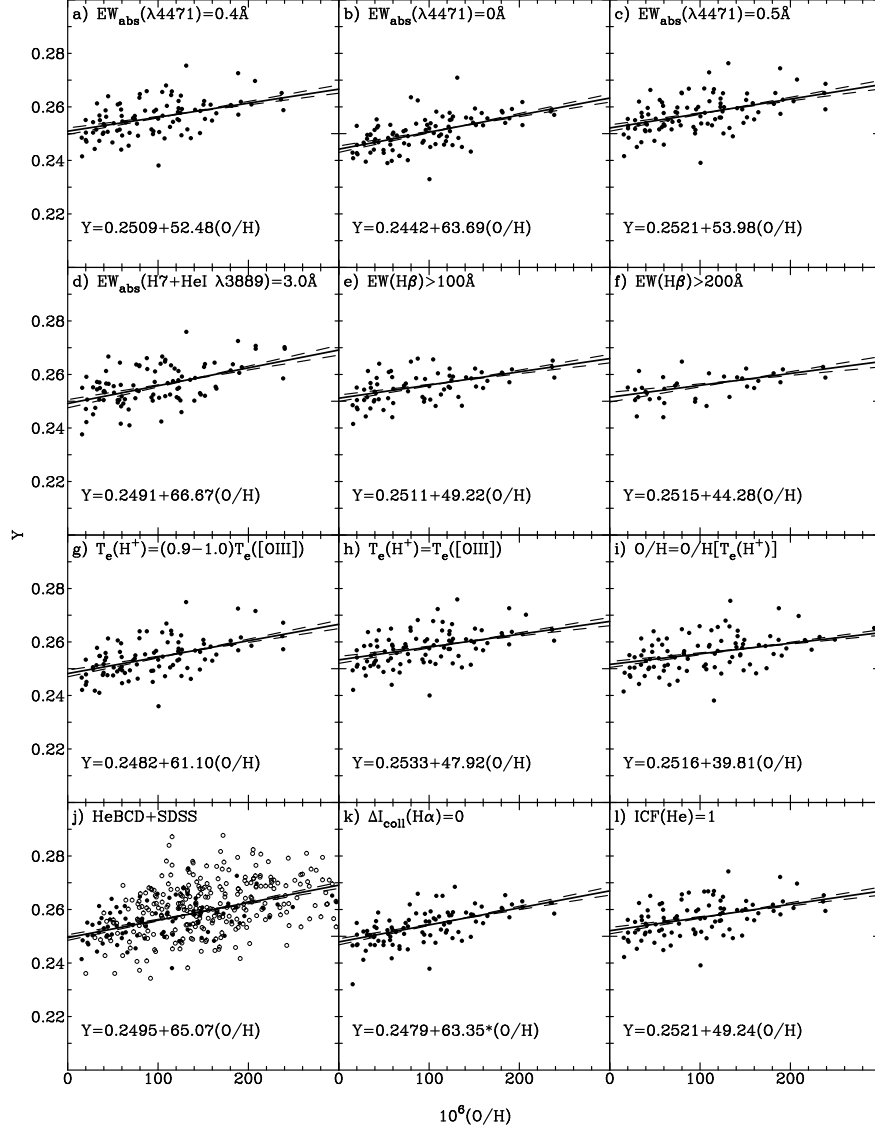


Fig. 3.— Linear regressions of the helium mass fraction  $Y$  vs. oxygen abundances for different parameter sets. The He I emissivities are from Porter et al. (2005). (a)  $Y$ s are derived for the HeBCD sample adopting  $EW_{abs}(\lambda 4471) = 0.4 \text{ \AA}$ . The electron temperature  $T_e(He^+)$  is varied in the range  $(0.95 - 1.0) \times T_e(O \text{ III})$  (basic model). (b) same as in (a), but for  $EW_{abs}(\lambda 4471) = 0.0 \text{ \AA}$ . (c) same as in (a), but for  $EW_{abs}(\lambda 4471) = 0.5 \text{ \AA}$ . (d) same as in (a), but for  $EW_{abs}(H7 + \lambda 3889) = 3.0 \text{ \AA}$  instead of  $EW_{abs}(\lambda 3889) = EW_{abs}(\lambda 4471)$ . (e) same as in (a), but only objects with  $EW(H\beta) \geq 100 \text{ \AA}$  are shown. (f) same as in (a), but only objects with  $EW(H\beta) \geq 200 \text{ \AA}$  are shown. (g) same as in (a), but  $T_e(He^+)$  is varied in the range  $(0.9 - 1.0) \times T_e(O \text{ III})$ . (h) same as in (a), but with  $T_e(He^+) = T_e(O \text{ III})$ . (i) same as in (a), but oxygen abundance  $O/H$  is derived adopting  $T_e(He^+)$  instead of  $T_e(O \text{ III})$ . (j) same as in (a), but adding the H II regions from the SDSS. (k) same as in (a), but for zero collisional excitation of hydrogen lines. (l) same as in (a), but the ionization correction factor  $ICF(He^+ + He^{2+})$  is set to 1.

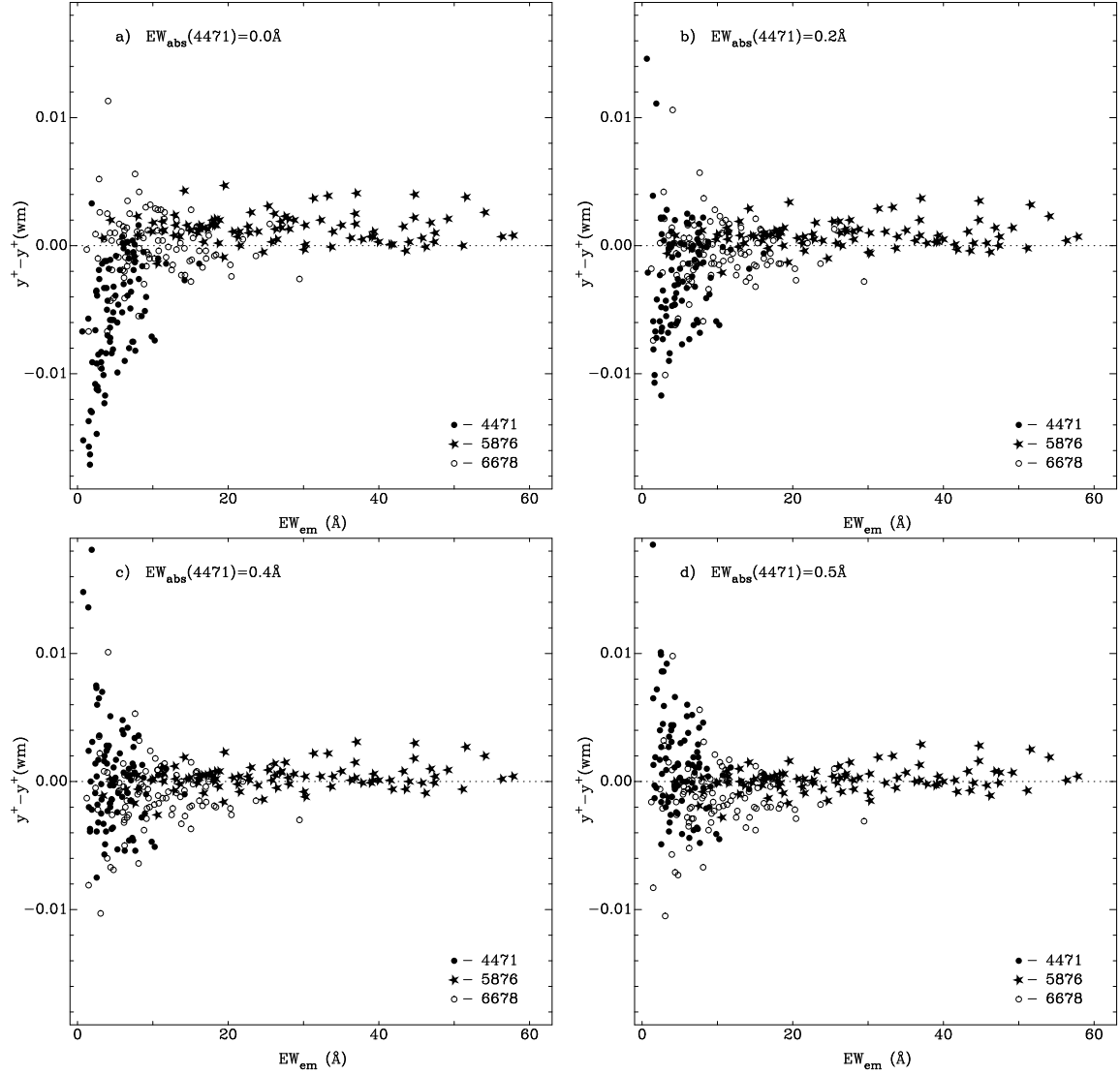


Fig. 4.—  $(y^+ - y_{wm}^+)$  derived for each of the three He I emission lines  $\lambda 4471$  (filled circles),  $\lambda 5876$  (stars) and  $\lambda 6678$  (open circles) vs the equivalent width  $EW_{em}$  of the same lines.  $y_{wm}^+$  is the weighted mean of the  $y^+$  of each individual line. Four different values of  $EW_{abs}(\lambda 4471)$  have been adopted: a)  $EW_{abs}(\lambda 4471) = 0$ , b)  $EW_{abs}(\lambda 4471) = 0.2 \text{ Å}$ , c)  $EW_{abs}(\lambda 4471) = 0.4 \text{ Å}$  and d)  $EW_{abs}(\lambda 4471) = 0.5 \text{ Å}$ . Only data for the HeBCD sample are shown.

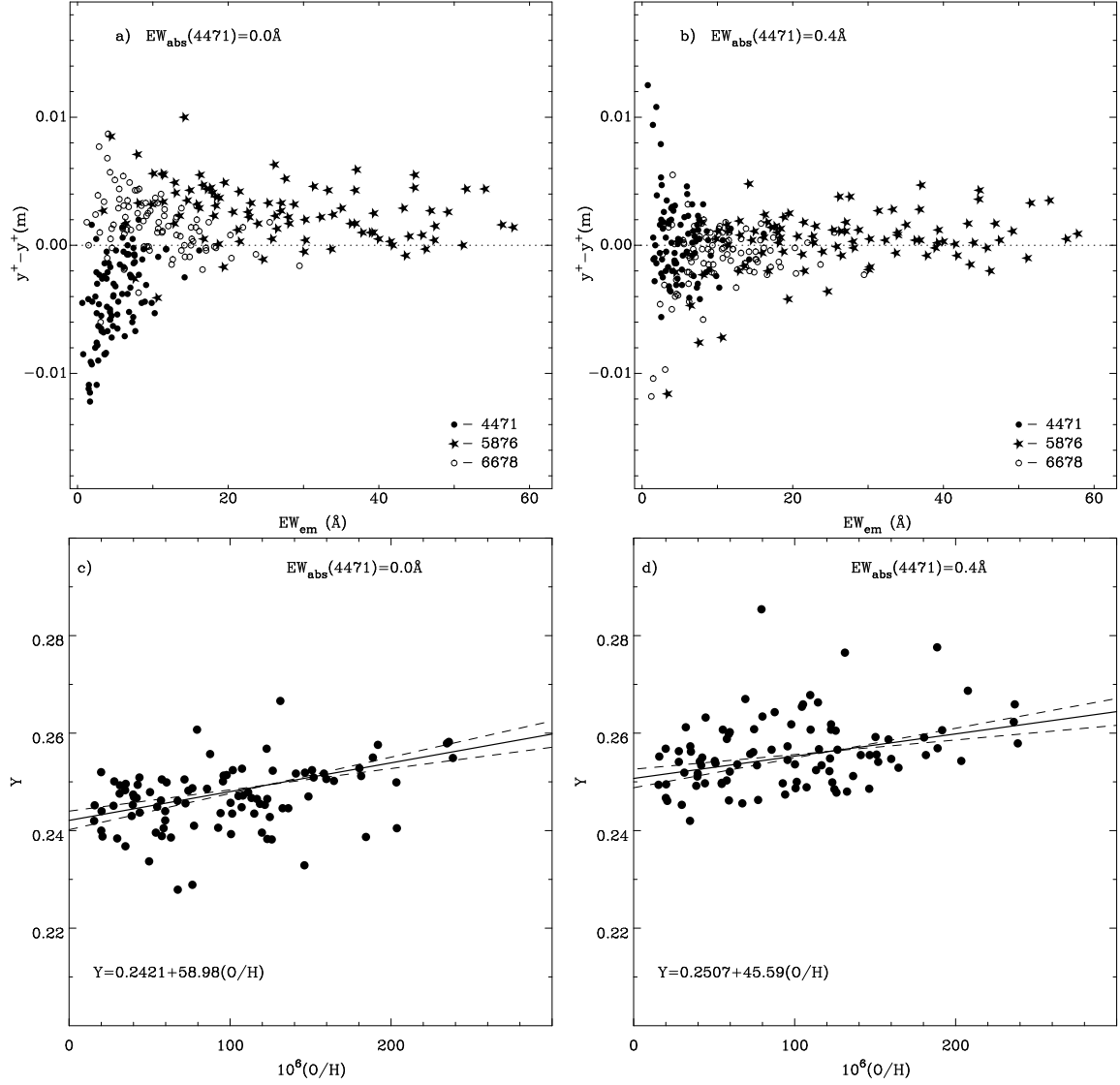


Fig. 5.— a) Same as in Fig. 4a, except that  $y_m^+$  is the simple mean instead of the weighted mean  $y_{wm}^+$ ; b) Same as in Fig. 4c, except that  $y_m^+$  is the simple mean instead of the weighted mean  $y_{wm}^+$ ; c) Same as in Fig. 3c, except that  $y_m^+$  is the simple mean instead of the weighted mean  $y_{wm}^+$ ; d) Same as in Fig. 3a, except that  $y_m^+$  is the simple mean instead of the weighted mean  $y_{wm}^+$ .

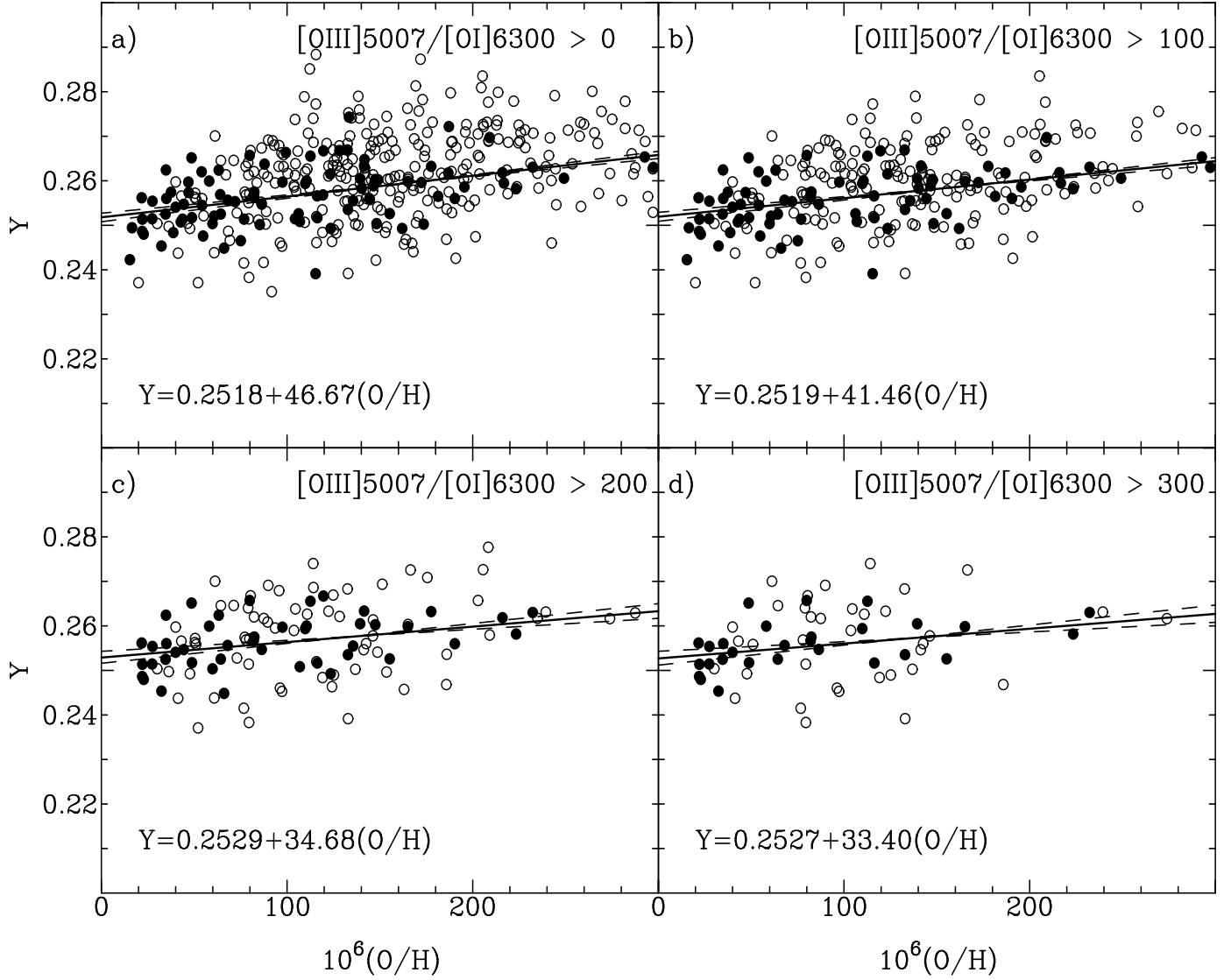


Fig. 6.— Linear regressions of the helium mass fraction  $Y$  vs. oxygen abundances for H II regions with different values of the  $[O\text{ III}]\lambda 5007/[O\text{ I}]\lambda 6300$  emission flux ratio. The He I emissivities are from Porter et al. (2005). The ionization correction factor  $ICF(\text{He}^+ + \text{He}^{2+})$  is set to 1. In panel a) all H II regions are shown, while in panels b), c) and d) are shown H II regions with the  $[O\text{ III}]\lambda 5007/[O\text{ I}]\lambda 6300$  emission flux ratio respectively greater than 100, 200 and 300.

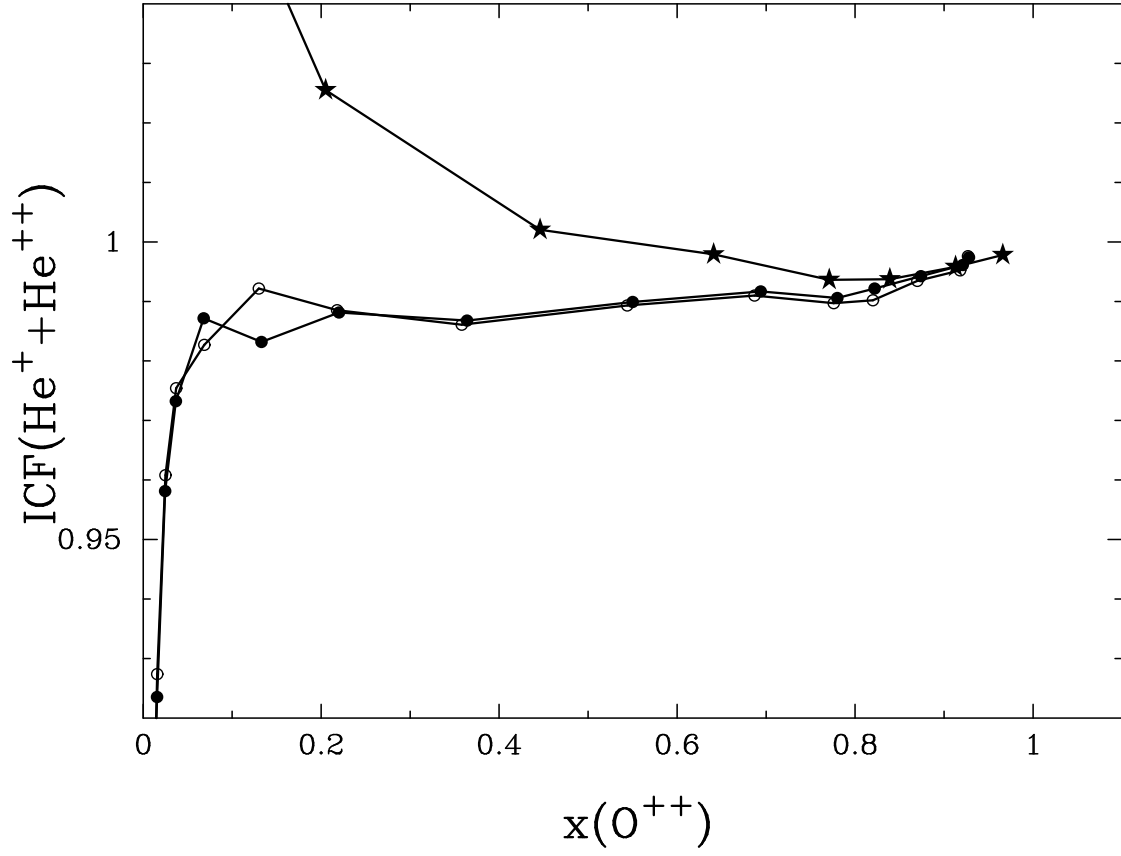


Fig. 7.— Ionization correction factor  $ICF(He^+ + He^{2+})$  as a function of the doubly ionized oxygen abundance fraction  $O^{2+}/(O^+ + O^{2+})$

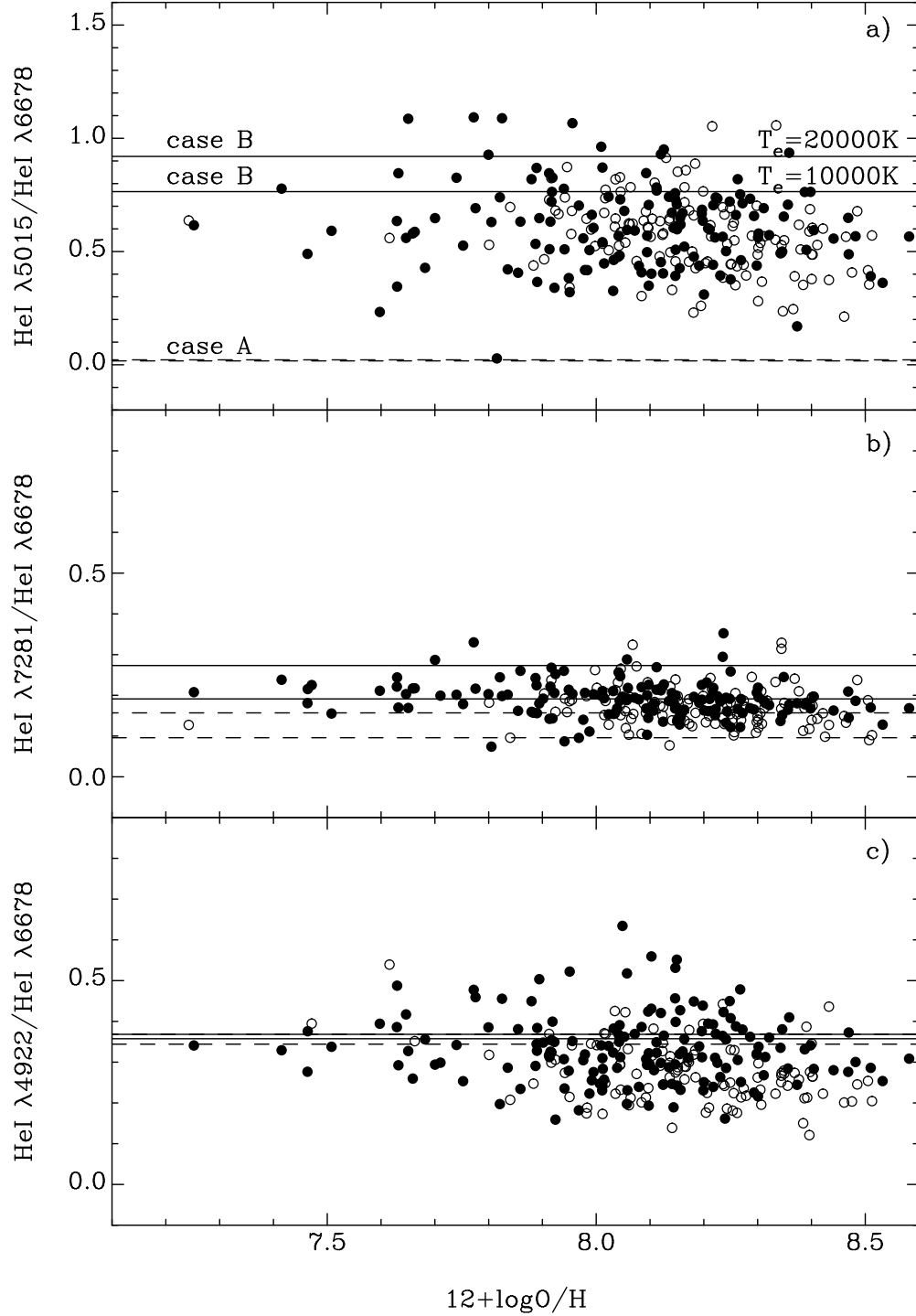


Fig. 8.— Flux ratios of singlet He I emission lines vs oxygen abundance for the SDSS H II regions. Filled circles are H II regions with  $\text{EW}(\text{H}\beta) \geq 100 \text{\AA}$  and open circles are H II regions with  $\text{EW}(\text{H}\beta) < 100 \text{\AA}$ . The flux ratios for cases A and B are shown respectively by dashed and solid horizontal lines.

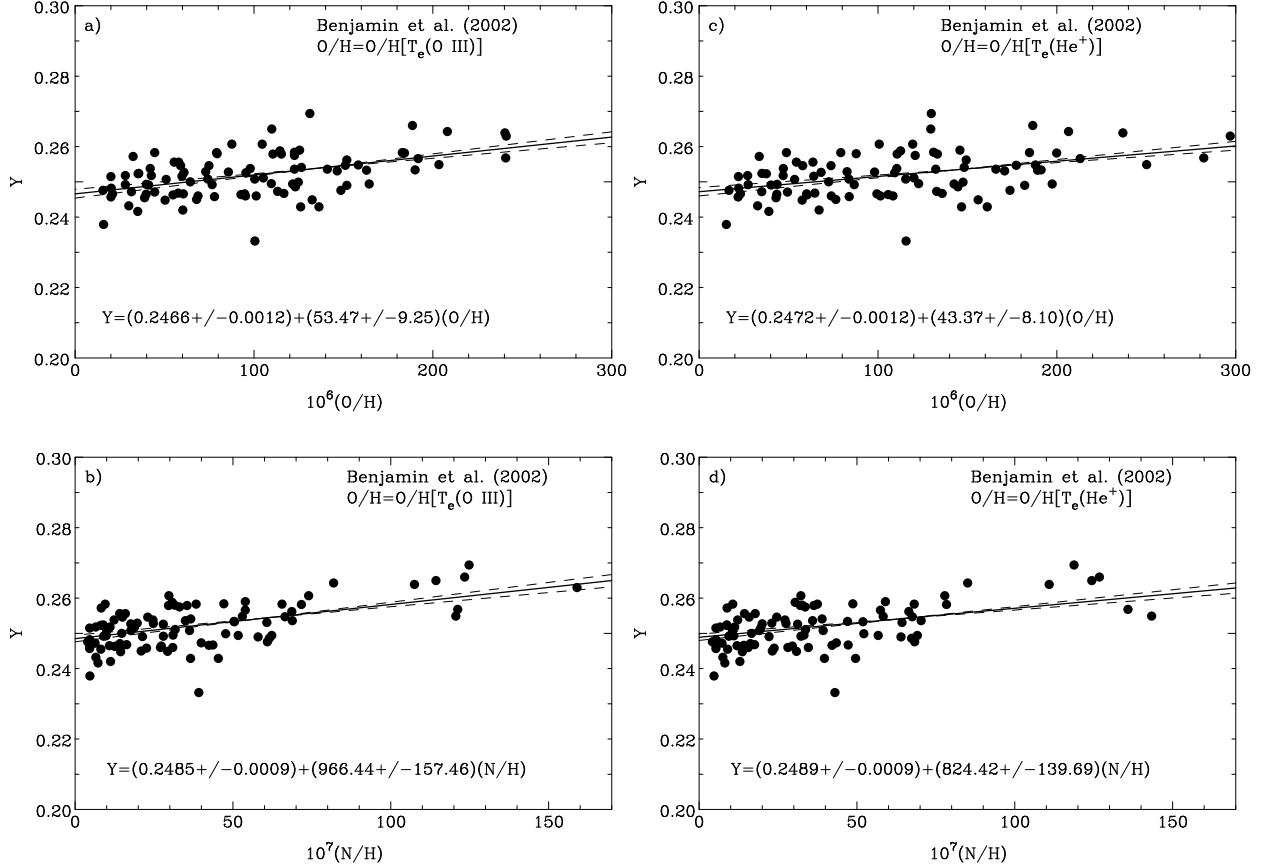


Fig. 9.— Linear regressions of the helium mass fraction  $Y$  vs. oxygen and nitrogen abundances for H II regions from the HeBCD sample. The  $Y$ s are derived with the He I emissivities from Benjamin et al. (1999, 2002). The electron temperature  $T_e(\text{He}^+)$  is varied in the range  $(0.95 - 1) \times T_e(\text{O III})$ . The oxygen abundance is derived adopting  $T_e(\text{O III})$  in a) and b) and  $T_e(\text{He}^+)$  in c) and d).

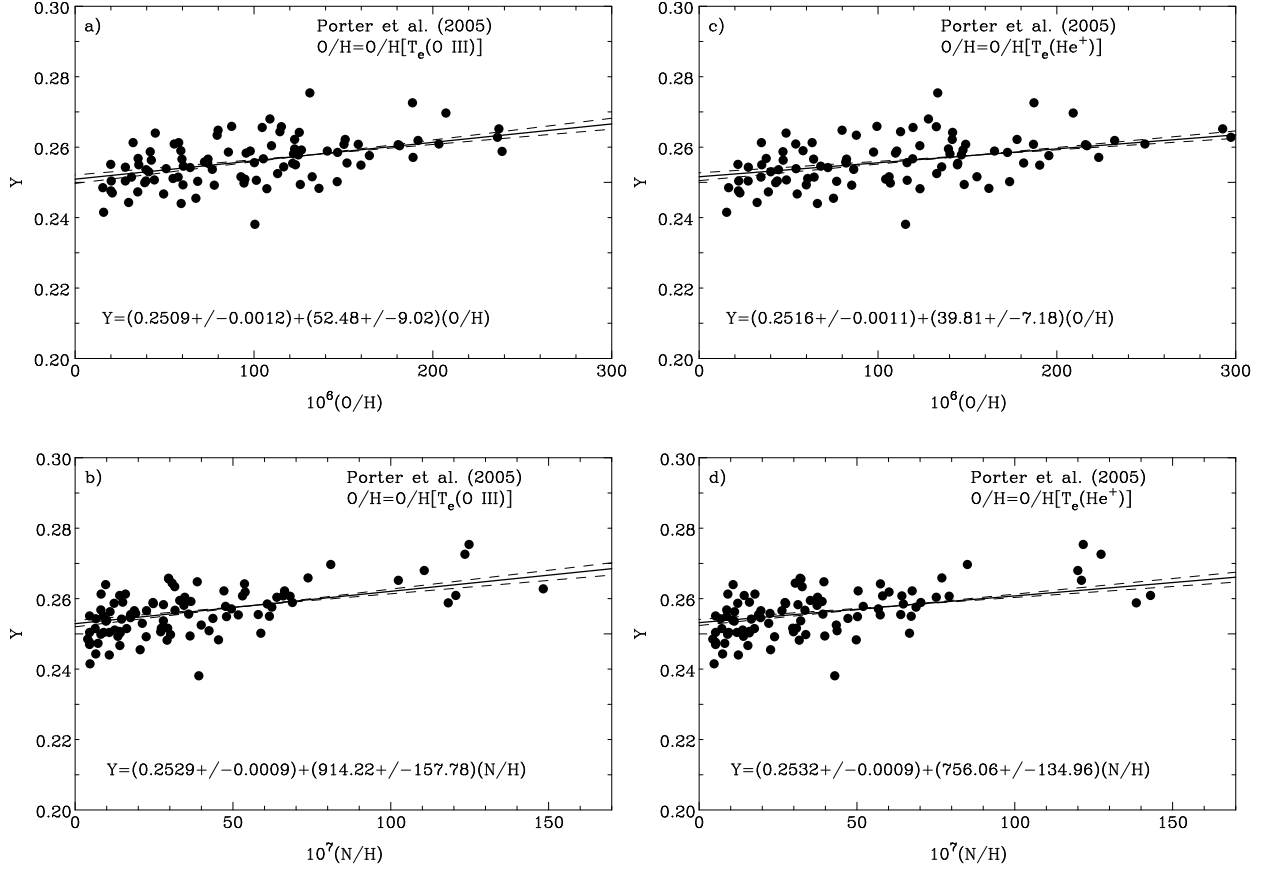


Fig. 10.— Same as in Fig. 9 but  $Y$ s are derived with the Porter et al. (2005) He I emissivities.



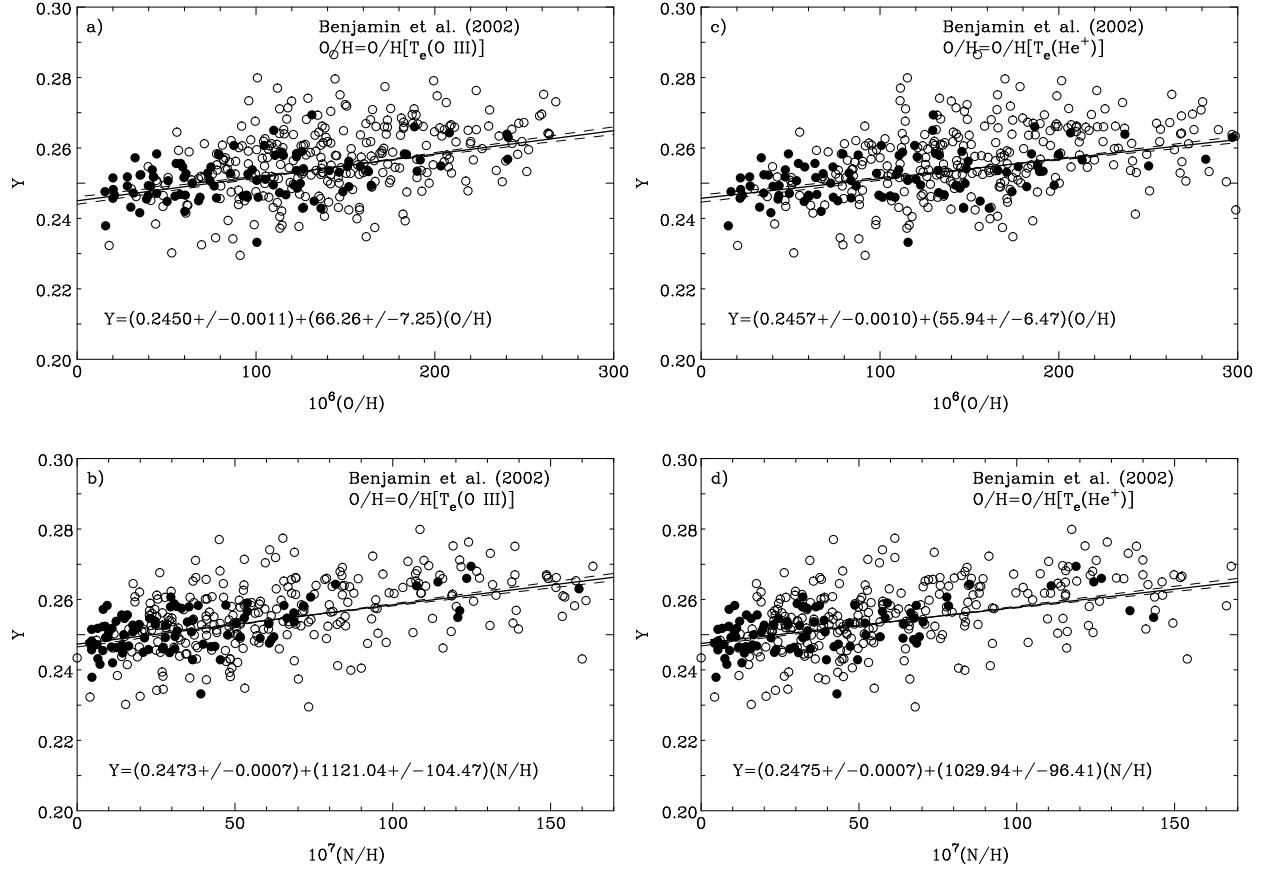


Fig. 11.— Same as in Fig. 9, but for the HeBCD + SDSS sample. HeBCD H II regions are shown by filled circles and SDSS H II regions by open circles.

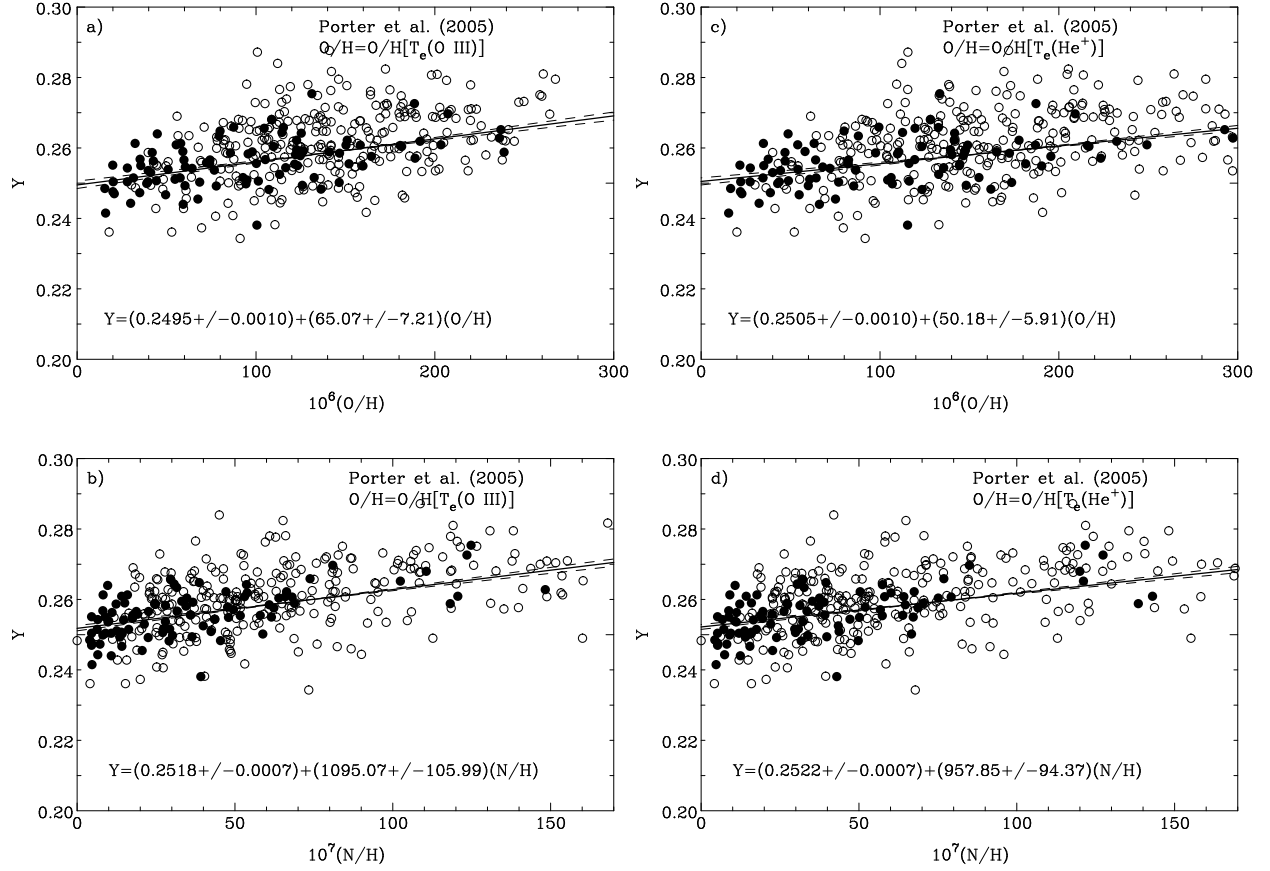


Fig. 12.— Same as in Fig. 10, but for the HeBCD + SDSS sample. HeBCD H II regions are shown by filled circles and SDSS H II regions by open circles.

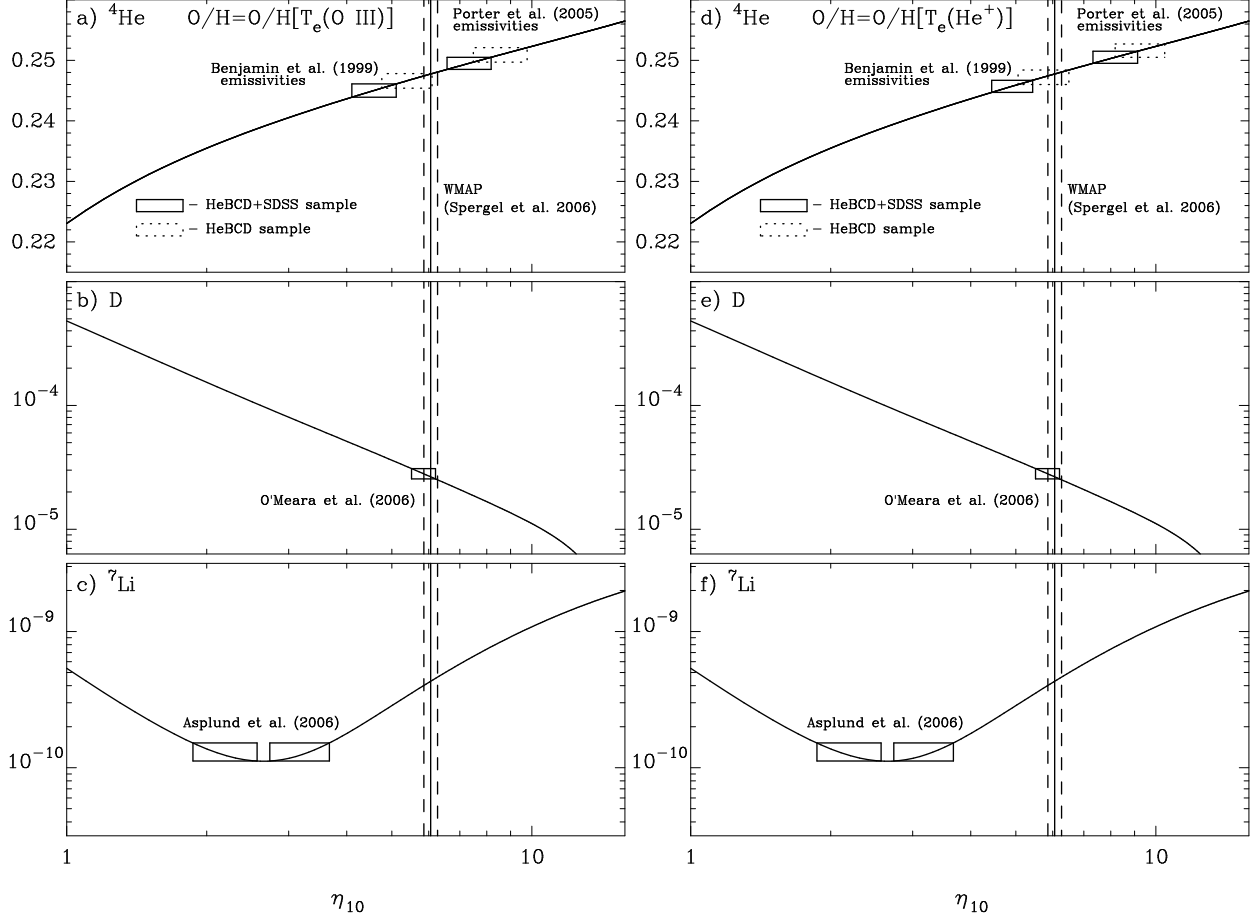


Fig. 13.— Dependence of the helium mass fraction (a),(d), deuterium (b),(e) and  $^7Li$  (c),(f) abundances on the photon-to-baryon number ratio  $\eta$ . Solid curves are predictions of the SBBN, solid and dashed vertical lines indicate the  $\eta$  and  $1\sigma$  deviations derived from WMAP (Spergel et al. 2006). Boxes show the observed light element abundances along with their  $1\sigma$  deviations. The solid boxes correspond to the combined HeBCD + SDSS sample and the dotted boxes to the HeBCD sample only. Boxes in (a) are calculated adopting  $O/H = O/H[T_e(O\ III)]$ , and boxes in (d) are calculated adopting  $O/H = O/H[T_e(He^+)]$ .

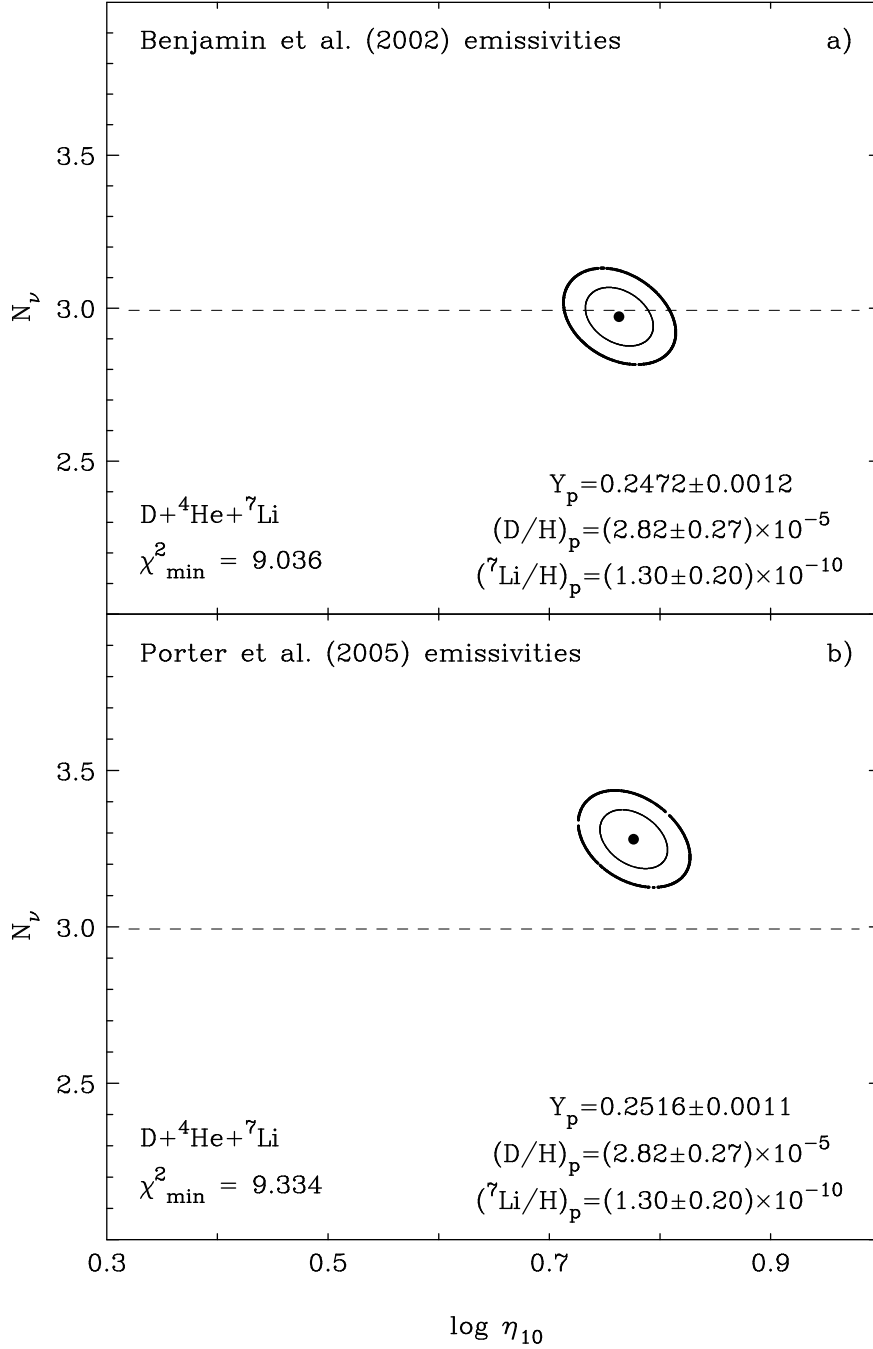


Fig. 14.— Joint fits to the baryon-to-photon number ratio,  $\log \eta_{10}$ , and the equivalent number of light neutrino species  $N_\nu$ , using a  $\chi^2$  analysis with the code developed by Fiorentini et al. (1998) and Lisi et al. (1999) (a) for the primordial abundance value  $Y_p$  derived with the Benjamin et al. (2002) He I emissivities (this paper),  $(D/H)_p$  from O’Meara et al. (2006) and  $({}^7\text{Li}/H)_p$  from Asplund et al. (2006) and (b) for the primordial abundance value  $Y_p$  derived with the Porter et al. (2005) He I emissivities (this paper), and the same  $(D/H)_p$  and  $({}^7\text{Li}/H)_p$  as in (a). Thin and thick solid lines are respectively  $1\sigma$  and  $2\sigma$  deviations. The experimental value  $N_\nu = 2.993$  (Caso et al. 1998) is shown by the dashed line.

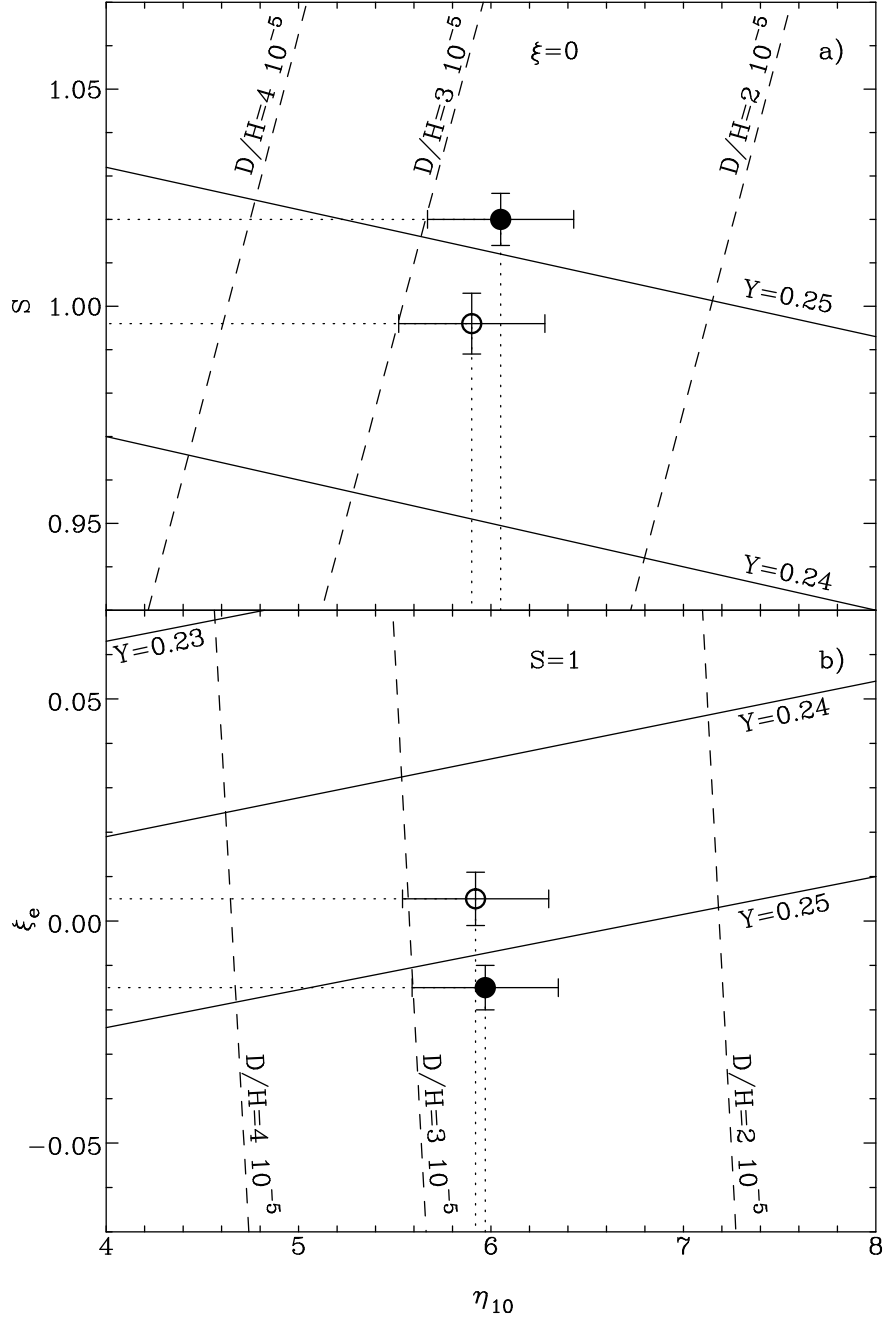


Fig. 15.— (a) Diagram showing the expansion rate factor  $S$  vs the baryon-to-photon number ratio  $\eta$ . Isoabundance curves for D and He are shown respectively by dashed and solid lines and labeled by the abundance values. The filled circle corresponds to the primordial D/H abundance from O’Meara et al. (2006) and the primordial He mass fraction derived in this paper with the Porter et al. (2005) emissivities. The open circle corresponds to the primordial D/H abundance from O’Meara et al. (2006) and the primordial He mass fraction derived in this paper with the Benjamin et al. (1999) emissivities. Error bars are  $1\sigma$  deviations. (b) Same as in (a) except the diagram shows the electron neutrino asymmetry parameter  $\xi_e$  vs the baryon-to-photon number ratio  $\eta$ .

Table 1. Emission line fluxes

Object <sup>a</sup>	[O II] 3727 [O III] 4363 [N II] 6583	H12 3750 He I 4471 He I 6678	H11 3771 He II 4686 [S II] 6717	H10 3797 H $\beta$ 4861 [S II] 6731	H9 3835 [O III] 4959 He I 7065	H8+He I 3889 [O III] 5007 [O II] 7320	H $\delta$ 4102 He I 5876 [O II] 7330	H $\gamma$ 4340 H $\alpha$ 6563
CGCG 007-025 (No. 1)	88.7 $\pm$ 1.4 11.9 $\pm$ 1.0 4.1 $\pm$ 1.0	2.8 $\pm$ 1.0 3.5 $\pm$ 1.0 3.6 $\pm$ 1.0	3.5 $\pm$ 1.0 1.3 $\pm$ 1.0 9.0 $\pm$ 1.0	4.3 $\pm$ 1.0 100.0 $\pm$ 1.0 6.9 $\pm$ 1.0	6.1 $\pm$ 1.0 185.8 $\pm$ 2.1 4.0 $\pm$ 1.0	17.6 $\pm$ 1.0 564.2 $\pm$ 5.7 1.6 $\pm$ 1.0	23.7 $\pm$ 1.1 12.2 $\pm$ 1.0 1.3 $\pm$ 1.0	47.0 $\pm$ 1.1 349.9 $\pm$ 3.7
CGCG 007-025 (No. 2)	135.2 $\pm$ 2.1 10.2 $\pm$ 1.1 5.3 $\pm$ 1.1	2.3 $\pm$ 1.2 3.4 $\pm$ 1.1 3.3 $\pm$ 1.1	3.4 $\pm$ 1.2 0.8 $\pm$ 1.1 13.3 $\pm$ 1.1	4.9 $\pm$ 1.2 100.0 $\pm$ 1.1 9.2 $\pm$ 1.1	6.8 $\pm$ 1.2 151.2 $\pm$ 1.9 3.0 $\pm$ 1.1	16.7 $\pm$ 1.2 463.4 $\pm$ 4.8 ...	24.9 $\pm$ 1.1 11.1 $\pm$ 1.1 ...	45.7 $\pm$ 1.2 325.7 $\pm$ 3.5
HS 0029+1748	72.0 $\pm$ 1.4 2.5 $\pm$ 1.0 23.7 $\pm$ 1.0	1.4 $\pm$ 1.1 3.9 $\pm$ 1.0 4.1 $\pm$ 1.0	1.6 $\pm$ 1.1 ... 18.7 $\pm$ 1.0	3.0 $\pm$ 1.1 100.0 $\pm$ 1.0 15.1 $\pm$ 1.0	3.9 $\pm$ 1.1 134.1 $\pm$ 1.7 3.5 $\pm$ 1.0	12.7 $\pm$ 1.1 413.4 $\pm$ 4.3 3.2 $\pm$ 1.0	18.7 $\pm$ 1.1 13.0 $\pm$ 1.0 2.8 $\pm$ 1.0	41.2 $\pm$ 1.1 347.7 $\pm$ 3.6
HS 0111+2115	240.9 $\pm$ 3.5 7.1 $\pm$ 1.1 7.4 $\pm$ 1.1	... 3.5 $\pm$ 1.1 4.1 $\pm$ 1.1	... 0.8 $\pm$ 1.1 13.8 $\pm$ 1.1	... 100.0 $\pm$ 1.0 10.3 $\pm$ 1.1	... 200.3 $\pm$ 2.3 3.3 $\pm$ 1.1	11.0 $\pm$ 1.5 609.6 $\pm$ 6.2 2.0 $\pm$ 1.1	18.1 $\pm$ 1.5 13.0 $\pm$ 1.1 1.4 $\pm$ 1.1	38.6 $\pm$ 1.5 381.8 $\pm$ 4.0
HS 0122+0743	66.7 $\pm$ 1.4 3.5 $\pm$ 1.4 27.5 $\pm$ 1.4	2.0 $\pm$ 1.1 3.7 $\pm$ 1.5 4.5 $\pm$ 1.4	2.8 $\pm$ 1.1 ... 36.1 $\pm$ 1.5	3.6 $\pm$ 1.1 100.0 $\pm$ 1.3 24.7 $\pm$ 1.5	6.0 $\pm$ 1.1 153.3 $\pm$ 2.2 4.4 $\pm$ 1.5	16.6 $\pm$ 1.1 476.4 $\pm$ 5.1 ...	23.1 $\pm$ 1.1 15.1 $\pm$ 1.4 ...	45.1 $\pm$ 1.2 413.5 $\pm$ 4.7
(Abridged. Table with all H II regions will be published in the online edition of ApJ)								

<sup>a</sup>The first 93 entries are HeBCD H II regions with names in alphabetical order. The remaining 271 entries are SDSS H II regions. Their names are in the format xxxxx-yyyy-zzz, where xxxxx is the middle Julian date (MJD) of the observation, yyyy is the plate number, and zzz is the fiber number.

Table 2. Emission line EWs

Object <sup>a</sup>	[O II] 3727 [O III] 4363 [N II] 6583	H12 3750 He I 4471 He I 6678	H11 3771 He II 4686 [S II] 6717	H10 3797 H $\beta$ 4861 [S II] 6731	H9 3835 [O III] 4959 He I 7065	H8+He I 3889 [O III] 5007 [O II] 7320	H $\delta$ 4102 He I 5876 [O II] 7330	H $\gamma$ 4340 H $\alpha$ 6563
CGCG 007-025 (No. 1)	127.8 $\pm$ 0.6 25.7 $\pm$ 0.2 15.7 $\pm$ 0.2	4.1 $\pm$ 0.3 8.1 $\pm$ 0.2 15.8 $\pm$ 0.3	5.1 $\pm$ 0.3 3.4 $\pm$ 0.2 40.4 $\pm$ 0.3	6.4 $\pm$ 0.3 270.2 $\pm$ 0.5 31.3 $\pm$ 0.3	9.1 $\pm$ 0.2 535.6 $\pm$ 0.6 20.4 $\pm$ 0.4	26.3 $\pm$ 0.3 1633.0 $\pm$ 1.1 9.1 $\pm$ 0.4	42.8 $\pm$ 0.2 47.4 $\pm$ 0.3 7.6 $\pm$ 0.4	100.4 $\pm$ 0.3 1544.0 $\pm$ 1.3
CGCG 007-025 (No. 2)	131.0 $\pm$ 1.1 16.5 $\pm$ 0.4 18.9 $\pm$ 0.6	2.4 $\pm$ 0.6 5.9 $\pm$ 0.4 12.1 $\pm$ 0.6	3.6 $\pm$ 0.5 1.6 $\pm$ 0.3 47.2 $\pm$ 0.8	5.2 $\pm$ 0.5 204.3 $\pm$ 0.8 34.2 $\pm$ 0.8	7.4 $\pm$ 0.4 308.8 $\pm$ 0.9 12.5 $\pm$ 0.8	21.7 $\pm$ 0.8 952.1 $\pm$ 1.5 ...	32.8 $\pm$ 0.4 34.0 $\pm$ 0.6 ...	72.3 $\pm$ 0.5 1152.0 $\pm$ 2.4
HS 0029+1748	106.3 $\pm$ 0.9 2.9 $\pm$ 0.1 62.4 $\pm$ 0.2	2.1 $\pm$ 0.6 4.8 $\pm$ 0.1 11.6 $\pm$ 0.1	2.3 $\pm$ 0.5 ... 51.6 $\pm$ 0.2	4.1 $\pm$ 0.4 153.0 $\pm$ 0.2 41.7 $\pm$ 0.2	5.3 $\pm$ 0.3 215.9 $\pm$ 0.2 10.6 $\pm$ 0.2	19.2 $\pm$ 0.3 681.9 $\pm$ 0.4 10.2 $\pm$ 0.2	24.3 $\pm$ 0.3 30.3 $\pm$ 0.1 8.7 $\pm$ 0.2	54.5 $\pm$ 0.3 919.1 $\pm$ 0.5
HS 0111+2115	117.8 $\pm$ 1.0 9.3 $\pm$ 0.2 15.5 $\pm$ 0.3	... 4.7 $\pm$ 0.2 8.7 $\pm$ 0.3	... 1.0 $\pm$ 0.2 29.5 $\pm$ 0.4	... 149.4 $\pm$ 0.4 22.0 $\pm$ 0.3	... 298.6 $\pm$ 0.6 7.8 $\pm$ 0.4	5.1 $\pm$ 0.4 912.1 $\pm$ 0.9 5.1 $\pm$ 0.5	8.8 $\pm$ 0.4 22.8 $\pm$ 0.3 3.4 $\pm$ 0.5	21.4 $\pm$ 0.4 793.9 $\pm$ 1.1
HS 0122+0743	103.1 $\pm$ 0.8 1.8 $\pm$ 0.3 23.9 $\pm$ 0.6	3.1 $\pm$ 0.4 2.0 $\pm$ 0.3 3.9 $\pm$ 0.5	4.3 $\pm$ 0.4 ... 32.4 $\pm$ 0.7	5.5 $\pm$ 0.4 63.0 $\pm$ 0.5 22.1 $\pm$ 0.6	9.1 $\pm$ 0.3 98.3 $\pm$ 0.6 4.2 $\pm$ 0.6	24.2 $\pm$ 0.4 307.0 $\pm$ 0.8 ...	38.7 $\pm$ 0.4 11.5 $\pm$ 0.4 ...	83.6 $\pm$ 0.5 357.9 $\pm$ 1.5
(Abridged. Table with all H II regions will be published in the online edition of ApJ)								

<sup>a</sup>The first 93 entries are HeBCD H II regions with names in alphabetical order. The remaining 271 entries are SDSS H II regions. Their names are in the format xxxxx-yyyy-zzz, where xxxxx is the middle Julian date (MJD) of the observation, yyyy is the plate number, and zzz is the fiber number.

Table 3. Oxygen, nitrogen and helium abundances for the best solutions with the Porter et al. (2005) He I emissivities

Object <sup>a</sup>	O/H <sup>b,d</sup>	O/H <sup>c,d</sup>	N/H <sup>b,e</sup>	N/H <sup>c,e</sup>	Y	EW(H $\beta$ )
CGCG 007-025 (No. 1)	6.0 $\pm$ 0.1	6.0 $\pm$ 0.1	13.5 $\pm$ 0.3	14.0 $\pm$ 0.3	0.2493 $\pm$ 0.0060	270
CGCG 007-025 (No. 2)	5.5 $\pm$ 0.2	6.1 $\pm$ 0.2	12.6 $\pm$ 0.5	13.8 $\pm$ 0.5	0.2511 $\pm$ 0.0069	204
HS 0029+1748	11.3 $\pm$ 0.4	13.3 $\pm$ 0.4	40.0 $\pm$ 1.4	43.5 $\pm$ 1.4	0.2525 $\pm$ 0.0043	149
HS 0111+2115	20.7 $\pm$ 2.8	20.9 $\pm$ 2.8	81.0 $\pm$ 8.7	85.0 $\pm$ 8.7	0.2697 $\pm$ 0.0100	63
HS 0122+0743	4.0 $\pm$ 0.1	4.4 $\pm$ 0.1	9.8 $\pm$ 0.4	11.1 $\pm$ 0.4	0.2536 $\pm$ 0.0055	232
<b>(Abridged. Table with all H II regions will be published in the online edition of ApJ)</b>						

<sup>a</sup>The first 93 entries are HeBCD H II regions with names in alphabetical order. The remaining 271 entries are SDSS H II regions. Their names are in the format xxxxx-yyyy-zzz, where xxxxx is the middle Julian date (MJD) of the observation, yyyy is the plate number, and zzz is the fiber number.

<sup>b</sup>Abundances are calculated adopting  $T_e=T_e(\text{O III})$ .

<sup>c</sup>Abundance are calculated adopting  $T_e=T_e(\text{He}^+)$ .

<sup>d</sup>In units  $10^{-5}$ .

<sup>e</sup>In units  $10^{-7}$ .

Table 4. Parameters for the best solution for He mass fraction in Table 3

Object <sup>a</sup>	$T_e(\text{O III})$	$T_e(\text{He}^+)$	$N_e$	$\tau(\lambda 3889)$	$\Delta\text{H}\alpha/\text{H}\alpha$	$ICF$	$\chi^2_{min}$
CGCG 007-025 (No. 1)	1.64 $\pm$ 0.02	1.64 $\pm$ 0.04	295 $^{+102}_{-51}$	0.75 $^{+0.16}_{-0.23}$	0.0144	0.9957	0.72E+00
CGCG 007-025 (No. 2)	1.65 $\pm$ 0.03	1.57 $\pm$ 0.04	13 $^{+96}_{-2}$	0.94 $^{+0.26}_{-0.59}$	0.0001	0.9963	0.21E+01
HS 0029+1748	1.28 $\pm$ 0.02	1.22 $\pm$ 0.03	12 $^{+47}_{-1}$	1.16 $^{+0.24}_{-0.36}$	0.0000	0.9959	0.78E+01
HS 0111+2115	1.11 $\pm$ 0.06	1.10 $\pm$ 0.03	459 $^{+1}_{-268}$	1.15 $^{+1.54}_{-0.59}$	0.0427	1.0000	0.43E+00
HS 0122+0743	1.76 $\pm$ 0.02	1.68 $\pm$ 0.05	11 $^{+66}_{-0}$	1.05 $^{+0.12}_{-0.50}$	0.0003	0.9957	0.29E+01
<b>(Abridged. Table with all H II regions will be published in the online edition of ApJ)</b>							

<sup>a</sup>The first 93 entries are HeBCD H II regions with names in alphabetical order. The remaining 271 entries are SDSS H II regions. Their names are in the format xxxxx-yyyy-zzz, where xxxxx is the middle Julian date (MJD) of the observation, yyyy is the plate number, and zzz is the fiber number.

Table 5. Budget of different systematics effects in the  $Y_p$  determination

Property	$\Delta Y_p$
He I emissivity	$\lesssim +1.7\%$
$T_e(\text{He}^+) = (0.95 - 1.0) \times T_e(\text{O III})$	$\lesssim -1.0\%$
Underlying He I stellar absorption	$\lesssim +3.0\%$
Collisional excitation of hydrogen emission lines	$\lesssim +1.0\%$
$ICF(\text{He}^+ + \text{He}^{2+})$	$\lesssim -1.0\%$

Table 6. Maximum Likelihood Linear Regressions

Method	$N$	Oxygen	Nitrogen
a) $O/H=O/H[T_e(O\ III)], N/H=N/H[T_e(O\ III)]$			
Old He I emissivities	93	$0.2466 \pm 0.0012 + 53 \pm 9(O/H)$	$0.2485 \pm 0.0009 + 966 \pm 157(N/H)$
Old He I emissivities	364	$0.2460 \pm 0.0011 + 66 \pm 7(O/H)$	$0.2473 \pm 0.0007 + 1121 \pm 104(N/H)$
New He I emissivities	93	$0.2509 \pm 0.0012 + 52 \pm 9(O/H)$	$0.2529 \pm 0.0009 + 914 \pm 158(N/H)$
New He I emissivities	364	$0.2495 \pm 0.0010 + 65 \pm 7(O/H)$	$0.2518 \pm 0.0007 + 1095 \pm 106(N/H)$
b) $O/H=O/H[T_e(He^+)], N/H=N/H[T_e(He^+)]$			
Old He I emissivities	93	$0.2472 \pm 0.0012 + 43 \pm 8(O/H)$	$0.2489 \pm 0.0009 + 824 \pm 140(N/H)$
Old He I emissivities	364	$0.2457 \pm 0.0010 + 56 \pm 6(O/H)$	$0.2475 \pm 0.0007 + 1030 \pm 96(N/H)$
New He I emissivities	93	$0.2516 \pm 0.0011 + 40 \pm 7(O/H)$	$0.2532 \pm 0.0009 + 756 \pm 135(N/H)$
New He I emissivities	364	$0.2505 \pm 0.0010 + 50 \pm 6(O/H)$	$0.2522 \pm 0.0007 + 958 \pm 94(N/H)$